

Spatiotemporal organization, regulation and functions of tractions during neutrophil chemotaxis

Myung Eun Shin¹, Yuan He¹, Dong Li¹, Sungsoo Na², Farhan Chowdhury², Yeh-Chuin Poh², Olivier Collin^{2,5}, Pei Su¹, Primal de Lanerolle³, Martin A. Schwartz⁴, Ning Wang², and Fei Wang^{1*}

¹Department of Cell and Developmental Biology and Institute for Genomic Biology, University of Illinois at Urbana-Champaign, Urbana, IL 61801, USA.

²Department of Mechanical Science and Engineering, University of Illinois at Urbana-Champaign, Urbana, IL 61801, USA.

³Department of Physiology and Biophysics, University of Illinois at Chicago, Chicago, IL 60612, USA.

⁴Departments of Microbiology, Cell Biology and Biomedical Engineering, University of Virginia, Charlottesville, VA 22908, USA.

⁵Current address: Functional Imaging of Transcription, UMR 8197, Institut de Biologie Ecole Normale Supérieure Paris, 75230 Paris, France

***Corresponding author:** Department of Cell and Developmental Biology, University of Illinois at Urbana-Champaign, 601 S. Goodwin Ave, Urbana, IL -61801, USA. Tel.: 217-333-5972; Fax: 217-244-1648; E-mail: feiwang@life.uiuc.edu

Running title: tractions in neutrophils during chemotaxis

Key words: tractions, integrin activation, adhesion, neutrophil chemotaxis

Abstract

Despite recent advances in our understanding of biochemical regulation of neutrophil chemotaxis, little is known about how mechanical factors control neutrophils' persistent polarity and rapid motility. Here, by using a human neutrophil-like cell line and human primary neutrophils, we describe a dynamic spatiotemporal pattern of tractions during chemotaxis. Traction is located at both the leading and the trailing edge of neutrophils, where they oscillate with a defined periodicity. Interestingly, traction oscillations at the leading and the trailing edge are out of phase with the tractions at the front leading those at the back, suggesting a temporal mechanism that coordinates leading edge and trailing edge activities. The magnitude and periodicity of tractions depend upon the activity of non-muscle myosin IIA. Specifically, traction development at the leading edge requires myosin light chain kinase (MLCK)-mediated myosin II contractility and is necessary for $\alpha 5\beta 1$ -integrin activation and leading edge adhesion. Localized myosin II activation induced by spatially activated small GTPase Rho and its downstream kinase p160-ROCK, as previously reported, leads to contraction of actin-myosin II complexes at the trailing edge, causing it to de-adhere. Our data identify a key biomechanical mechanism for persistent cell polarity and motility.

Introduction

Chemotaxis – the directed movement of cells in a gradient of chemoattractant – is essential for neutrophils to crawl to sites of inflammation and infection. Chemoattractant-induced activation of spatially localized cellular signals causes neutrophils to initiate polymerization of actin at the leading edge (pseudopod), polarize (i.e., adopt an asymmetric shape with defined front and back) and move towards the highest concentration of the chemoattractant. Recent studies have begun to reveal some fascinating details of the intracellular biochemical components that spatially direct the neutrophils' cytoskeleton and the complex signaling pathways that control formation of their front and back ¹⁻⁴. Divergent frontness and backness signals provide a mechanism for neutrophils to polarize in uniform concentrations of chemoattractant and to perform U-turns rather than simply reverse polarity in response to changes in the direction of the attractant gradient ⁴.

Despite these findings, there are significant gaps in our understanding of the mechanical functions that control the persistent and rapid movement of neutrophils. Specifically, there is limited documentation of quantitative analysis of tractions in neutrophils, and the spatial and temporal dynamics, regulation and functions of tractions remain largely undefined. It is well established that slow moving cells such as fibroblasts assemble transient adhesions called focal complexes at the leading edge, which mature into more stable focal adhesions ⁵. Focal adhesions provide robust anchors to the extracellular matrix (ECM), allowing actomyosin-based stress fibers to pull the cell body forward. Traction are transmitted to the substrate at the site of focal adhesions and are required for maturation of these adhesion structures ⁶. In contrast, focal adhesions and stress fibers are not detected in migratory neutrophils or T cells ^{4,7}, raising the question whether and how mechanical forces control adhesion and directional migration in these rapidly moving amoeboid cells.

In this study, we revealed a highly dynamic spatiotemporal pattern of tractions in neutrophils during chemotaxis. The pattern is conserved in a human neutrophil-like cell line and primary human neutrophils and depends on non-muscle myosin IIA. We show that spatiotemporal organization of tractions requires localization-specific myosin II activation and is essential for leading edge adhesion and trailing edge de-adhesion. These data reveal a biomechanical mechanism that promotes the rapid and highly coordinated movements in neutrophils during chemotaxis.

Materials and Methods

Cell culture and transfection

Cultivation and differentiation of HL-60 cells were as described ². For transient transfections, the AMAXA nucleofection system was used. Differentiated HL-60 cells (2×10^7 , on day 5–6 after DMSO addition) were spun down and resuspended in nucleofector solution V. DNA (5 μ g) or siRNA (3 μ g) was added to the cells, and the cell-DNA mixture was subjected to nucleofection (program T-19). Nucleofected cells were transferred to 20 ml of complete medium. Subsequent assays were performed 3–6 h for the expression vectors and 24–48 h for siRNAs after transfection.

Isolation of primary neutrophils

Primary neutrophils were isolated from venous blood from healthy human donors. Blood was collected into heparin-containing Vacutainer tubes (BD Biosciences) and neutrophil isolation procedure was performed within 30 min of blood collection using PMN isolation medium (Matrix). Red blood cell contaminants were removed by Red Blood Cell Lysis buffer (Roche), which produced more than 97% of neutrophil purity. Neutrophils were suspended in RPMI 1640 medium supplemented with 10% fetal bovine serum at 37°C until the time of experiments conducted within 8 h after isolation.

Immunofluorescence and live-cell imaging

For immunofluorescence in fixed cells, cells were stimulated with 1 μ M fMLP in modified HBSS buffer (mHBSS) for the indicated time. Cells were extracted with 0.2% Triton X-100 for 10 min at room temperature (RT), fixed in 3.7% paraformaldehyde and immunostained. Antibodies were used at a dilutions of 1:50 (MLCK), 1:200 (p-MRLC), 1:500 (myosin heavy chain IIA), and 1:250 (α 5-

integrin), and immunostaining was performed as described ². F-actin was assessed by incubation of cells with 0.2 unit of Alexa Fluor 488 conjugated phalloidin (10 min, RT).

For live-cell imaging, cells were plated on human fibronectin-coated surface and stimulated either with a uniform concentration of 1 μ M fMLP or a point source of 10 μ M fMLP from a micropipette (internal diameter of 1 μ m, pulled from a glass capillary), as described ⁸. Differential interference contrast (DIC) images, fluorescent images and combined DIC/fluorescence images were collected with a Zeiss 40X NA 1.30 Fluar DIC objective or a 63X NA 1.4 Plan Apochromat DIC objective on a Zeiss Axiovert 200M microscope. All images were collected with a cooled charge-coupled device camera (AxioCam MR3, Zeiss) and processed by Image J.

For TIRF microscopy, a TIRF module based on Axiovert 200M microscope (Zeiss) was used as a starting point. Before each experiment, 488-nm excitation light from a 100-mW multiline argon-ion laser (Zeiss) was aligned properly to create evanescent wave that can only excite the molecules within a layer of 100 nm above the cover glass. At the start of an experiment, a fibronectin-coated cover glass to which cells were attached was placed on α Plan-Fluar 100x /1.45 oil objective lens. Microscopic images from the TIRF-illuminated cells were captured by AxioCam MR3 camera with an interval of 5 sec. Exposure times for each image were typically less than 1 sec, and the TIRF laser was shuttered with a Uniblitz COM2 shutter between exposures to minimize photodamage and photobleaching effects.

Polyacrylamide gel substrates, traction force microscopy (TFM) and data analysis

Polyacrylamide gels were prepared as described ⁹. Red fluorescent microspheres (0.2 μm , Molecular Probes) were embedded in gels for traction detection, and the gels were coated with 10 $\mu\text{g/ml}$ human fibronectin. The elastic Young modulus of the polyacrylamide gels was 3.5 kPa (5% acrylamide; 0.10% bis-acrylamide) ^{10,11}. 100-kPa gels were generated as described by Oakes *et al* ¹². Briefly, differentiated HL-60 (dHL-60) cells or primary neutrophils (1.0×10^5) with or without various treatments were allowed to adhere to the fibronectin-coated polyacrylamide gel for 10 min and migrate toward the micropipette containing 10 μM fMLP. TFM was performed using Andor Technology Revolution System Spinning Disk Confocal Microscopy system (Andor) coupled to an Olympus IX71 inverted microscope with Olympus 100x APO/1.4 NA objective. The working distance of the objective is ~ 0.13 mm. HL-60 cells stably expressing GFP were used for TFM to track the outline of cells during the migration. Primary neutrophils were labeled with calcein AM (30 min) or DiO (5 min) and washed once with RPMI 1640 media prior to imaging studies. 532 (20 mW) and 635 (25 mW) nm diode-pumped solid state (DPSS) laser lines were used to excite the fluorophores within the cell and the beads. The exposure time for both channels was 21 msec. Using iXon EM+ DU-897 back illuminated EMCCD (Andor Technology), images of cells expressing GFP and fluorescent beads were captured interchangeably every 0.8 sec for each fluorescent channel during stimulation and after cell detachment from the substrate. Images of the beads were analyzed by a custom-made program to calculate bead displacement and to generate traction maps. Images of beads after cell detachment, therefore traction-free, were used as a reference.

For traction analysis, the leading edge of a polarized neutrophil was defined as the area within the first 3 μm of the cell (for control cells and cells treated with Y-27632), while the rest of the cell was

defined as the trailing edge. For ML-7-treated, MLCK-depleted or blebbistatin-treated cells, the leading edge was defined as the area within the first 2.2 μm of the cell. These definitions were based upon quantifications of the leading-edge areas in HL-60 cells expressing the frontness markers such as YFP-actin and primary neutrophils stained with fluorescent phalloidin (for F-actin) with or without the drug treatments or MLCK depletion. The average tractions at the leading and trailing edges were calculated from the traction maps generated by the use of TFM.

To determine the periodicity of the front and rear tractions, Fourier analysis was performed using the traction values obtained from the TFM. The analysis was done using the built-in MATLAB “fft” (Fast Fourier Transform) function to transform the original time-domain traction signals into frequency domain. The PSD plots were then generated based on the results from the Fourier transform analysis.

To analyze cross correlation between tractions at the leading and trailing edges and to calculate the cross-correlation coefficient (r)¹³, a customized MATLAB (Mathworks) program was developed:

$$r = \frac{\sum_i (F_i - \bar{F})(B_i - \bar{B})}{\sqrt{\sum_i (F_i - \bar{F})^2 \sum_i (B_i - \bar{B})^2}},$$

where F_i and B_i are the mean traction values of the front and back at time point i , and \bar{F} and \bar{B} are the averaged mean traction values of the front and back over entire time. To examine the time lag between tractions at the leading and trailing edges, the values for tractions at the front were shifted in time with those at the back fixed.

Integrin activation assay

A GST-tagged protein composed of 9th, 10th, and 11th fibronectin (FN) type III repeats (denoted as GST-FN III₉₋₁₁) was used to monitor active $\alpha 5 \beta 1$ integrin as reported ¹⁴. The GST-FN fragment binds to unoccupied active integrins only. For adherent cells, integrin activation was determined as follows. After exposure to chemoattractant or buffer, cells were fixed with paraformaldehyde (3.7%) and incubated with 50 μ g/ml GST-FN III₉₋₁₁ in PBS with 1 mM Ca²⁺/1 mM Mg²⁺ at 37°C for 30 min. Because the GST-FN fragment competes with the FN substrate to an extent, fixation of cells could eliminate interference from the FN substrate. After incubation with GST-FN III₉₋₁₁, cells were gently washed, lysed in SDS sample buffer, and bound GST-FN III₉₋₁₁ was blotted with an anti-GST antibody (1:1000). For immunofluorescence studies, after fixation cells were incubated with GST-FN III₉₋₁₁, followed by incubation with GST antibody and Alexa-conjugated secondary antibody. For suspended cells, a similar procedure was used, except that the cells were not fixed. A rabbit anti- $\alpha 5$ integrin antibody (1:1000) was used to assess the total level and localization of $\alpha 5$ integrin.

Methods for other experimental procedures are available in the **Supplementary Methods**.

Results

Spatial and temporal organization of tractions during neutrophil chemotaxis

To assess the spatial and temporal pattern of tractions in neutrophils during chemotaxis, we plated cells on a flexible substrate coated with fibronectin and stimulated them with a point source of the chemoattractant formyl-Met-Leu-Phe (fMLP). Fibronectin has been widely used as a substrate for the study of neutrophil chemotaxis^{2,12,15}. We used a substrate stiffness of 3.5 kPa, resembling the stiffness of tissue cells such as endothelial cells (1-5 kPa)¹⁶. We used both the neutrophil-like differentiated HL-60 (dHL-60) cells and human primary neutrophils. HL-60 cells, when differentiated, exhibit neutrophil-like morphologies, polarize and migrate in gradients (or in uniform concentrations) of attractants at rates comparable to those of neutrophils from peripheral blood, but unlike primary neutrophils they can be continuously cultured and are genetically tractable^{2,4,8}. Therefore, HL-60 cells have been used widely as a model for studying neutrophil polarity and chemotaxis¹⁷⁻²⁰. We detected tractions at both the leading and the trailing edge of dHL-60 cells (Figure 1A). Tractions were not distributed evenly at the leading or the trailing edge but instead were often concentrated in small regions that ranged from 1 to 4 μm in diameter (Figure 1A; Supplementary Movie S1). Time-course analysis of tractions in cells moving towards fMLP revealed a highly dynamic temporal pattern: the mean level of tractions at both edges oscillated during migration (100-400 Pa) (Figure 1A-1B and Figure S1A) (The average tractions are summarized in Table 1). Fast-Fourier transform (FFT) analysis of the time-domain signals revealed periodicity of tractions in chemotaxing dHL-60 cells: the Power Spectral Density (PSD) plots of results from FFT analysis demonstrated a single pronounced peak at 4.8 ± 1.4 sec for tractions at the leading edge and 4.8 ± 1.6 sec for those at the trailing edge (means \pm SEM, n=9 cells) (Figure 1C and Figure S1B). Primary human neutrophils showed a similar pattern of tractions. Tractions were detected at both edges, where they oscillated at a periodicity of 4.7 ± 1.5 sec

and 4.7 ± 1.2 sec, respectively (means \pm SEM, n=6 cells) (Figure 1D). Interestingly, oscillations of tractions at the two edges were out of phase (Figure 1A and Figure S1A), and the tractions at the front preceded those at the back by 0.80 ± 0.23 sec [mean \pm SEM (n=9 cells); $p < 0.0001$] for dHL-60 cells and 0.40 ± 0.16 sec [mean \pm SEM (n=6 cells); $p < 0.001$] for primary cells, as shown by a cross-correlation analysis, which computed the time offsets between tractions at the front and the back by shifting the two data sets relative to each other (Figure 1E and 1F). The conserved periodic and out-of-phase behavior of tractions at the neutrophil's front and back suggests a biomechanical mechanism that drives coordinated movements of neutrophils via differential contractile stresses exerted onto the substrate.

Myosin II controls tractions and is required for neutrophil chemotaxis

Myosin II filaments can apply forces to move actin filaments relative to each other. During fibroblast migration, the contractile force generated by the actin-myosin cytoskeleton causes tractions on the underlying substrate by propagating through the actin-integrin-ECM link ²¹. We therefore assessed myosin II expression and spatial localization in neutrophils. Experiments with isoform-specific antibodies demonstrated that both dHL-60 cells and primary neutrophils mainly expressed myosin IIA (Figure S2A), consistent with an earlier report ²². We then assessed the spatial localization of myosin II using antibodies against total myosin IIA, myosin regulatory light chain (MRLC) phosphorylated at Ser19 [p[19]-MRLC ⁴, the activated form of MRLC] and an mCherry-tagged myosin IIA (mCherry-myosin IIA) ²³ in fixed or live dHL-60 cells. Both total and activated myosin II and the mCherry-tagged fusion protein were located mostly at the trailing edge of polarized neutrophils (69%, 68% and 72% of total fluorescence intensity for myosin IIA, p[19]-MRLC and mCherry-myosin IIA, respectively) (Figure 2A and 2B; Supplementary Movies S2 and S3), consistent with earlier reports ^{4,24}.

There was a considerable amount of myosin IIA localization at the front (31%, 32%, and 28%, respectively; Figure 2A and 2B), as described previously in studies in primary neutrophils^{15,25}. Using confocal fluorescence microscopy combined with 3D reconstruction, we found that myosin IIA was enriched around the periphery of the uropod (trailing edge) and distributed vertically and somewhat diffusely in the pseudopodia (Figure S2B; Supplementary Movies S4 and S5). Interestingly, although F-actin was highly enriched at the leading edge, it was also detected throughout the periphery of the cell including at the back of the cell (Figure S2B; Supplementary Movies S4 and S5).

We next impaired the function of myosin II in neutrophils and assessed the effect on tractions. As expected, inhibiting myosin II with blebbistatin (a specific myosin II inhibitor) in dHL-60 cells and primary neutrophils substantially reduced the tractions at both the leading and the trailing edge by up to 50% (Figure 2C and 2D) (Table 1). Remarkably, myosin II inhibition abolished the periodicity of tractions at both edges: myosin II-inhibited cells no longer exhibited periodic oscillations of tractions but instead showed random fluctuations, as shown by the lack of distinct frequencies/periods in all cells analyzed (n=10 for dHL-60 cells; n=6 for primary neutrophils) (Figure 2E and Fig. S2C-2D). Thus, myosin II is necessary for development and periodicity of tractions in neutrophils and serves as the molecular basis for tractions in neutrophils during chemotaxis.

Inhibition or depletion of myosin II also impaired neutrophil directional migration. In the presence of an fMLP gradient delivered by the micropipette, both dHL-60 cells and primary neutrophils, when plated on fibronectin-coated cover glass, polarized and rapidly migrated in the direction of the pipette with well-developed pseudopodia (Figure 2F and Fig. S5A; Supplementary Movie S6). In contrast, cells treated with blebbistatin failed to persist in forward movement and formed poorly-developed

unstable leading edges (Figure 2F; Supplementary Movie S7; data not shown). Differential interference contrast (DIC) kymographs of cells responding to the pipette stimulation demonstrated that blebbistatin-treated cells often retracted their leading edges after initial protrusion while untreated cells exhibited a persistent and progressive pattern of leading-edge protrusion (Figure 2G and Figure S3A-3H). In addition, blebbistatin treatment caused defects in contractility at the back of the cells, which in many cases exhibited long, stretched tails (Figure 2F, Figure S3D and Figure S3H), as previously reported ⁴. Differentiated HL-60 cells in which myosin IIA was depleted by small hairpin (sh)RNAs exhibited similar (albeit less profound) defects (Figure 2F-2G, Figure S3A-3D and Figure S3I; Supplementary Movie S8). Thus, myosin II inhibition (or depletion) caused neutrophils to form unstable leading edges and long tails. In contrast, inhibition of p160-ROCK, a key component of the previously documented “backness” pathway that regulates neutrophil polarity and chemotaxis ^{3,4}, reduced the level of activated myosin II at the back (Figure 3D), induced neutrophils to form long stretched tails (Figure 2F) ²⁶, but failed to affect protrusion of the leading edge (Figure 2F, 2G and Figure S3A-3H; Supplementary Movie S9). The backness pathway promotes localized activation of Rho and its downstream kinase p160-ROCK, leading to spatial activation of myosin II at the trailing edge ^{3,4}. Based on the differential effects of myosin II and p160-ROCK inhibition on protrusion, we inferred that myosin II activity at the neutrophil’s leading edge is necessary for stabilizing the protrusion response.

MLCK regulates leading edge stability, myosin II activity and tractions

We next explored how localization-specific myosin II activity and tractions were controlled at the leading and the trailing edge. Earlier studies demonstrated that the spatial activation of myosin II at the trailing edge is dependent on p160-ROCK and necessary for tail retraction and de-adhesion^{3,4}. We thus sought to understand how myosin II was spatially activated at the leading edge in neutrophils. MLCK, a $[Ca^{2+}]$ /calmodulin-dependent kinase, phosphorylates MRLC and induces contractility in multiple processes²⁷, including cell motility^{28,29}. To ask whether MLCK spatially regulated myosin II activation at the leading edge of neutrophils, we first examined its expression and subcellular localization. Western blotting indicated that both primary human neutrophils and dHL-60 cells mainly expressed the ~130-kD short form of MLCK (Supplementary Text and Figure S4A). In non-stimulated neutrophils, MLCK was diffusely distributed in the cytosol, with some cortical localization (Figure 3A). When stimulated with fMLP, it was recruited to the leading edge of polarized cells and co-localized with F-actin (Figure 3A). The polarized recruitment was confirmed by ectopic expression of EGFP-tagged short form MLCK (sMLCK-EGFP) (in accordance with its expression in neutrophils) (Supplementary Text and Figure S4B and S4C; Supplementary Movies S10 and S11). MLCK inhibition by a specific inhibitor ML-7 (25 μ M) impaired the stability of the leading edge and markedly reduced the speed of protrusion of dHL-60 cells and primary neutrophils, as shown by experiments with the micropipette assay (Figure 3B-3C; Figure S5). Similar to myosin II inhibition, MLCK inhibition caused neutrophils to often retract their leading edges during migration (\sim 0.4/min and 0.03/min for treated and untreated dHL-60 cells, respectively; \sim 0.7/min and 0.15/min for treated and untreated primary cells, respectively). However, unlike myosin II inhibition, MLCK inhibition failed to induce formation of stretched tails at the back of the cells (Fig. 3B and Fig. S5A).

In circulating neutrophils β 2-integrins are highly expressed and mediate the interactions with the endothelial cells. We thus assessed whether MLCK was also required for chemotaxis of neutrophils stimulated on ECM substrates for β 2-integrins. Differentiated HL-60 cells, when stimulated by a fMLP gradient on fibrinogen or Inter-Cellular Adhesion Molecule 1 (ICAM-1) (Figure S6 and data not shown), rapidly polarized and migrated towards the source of the chemoattractants (Figure S6). ML-7 treatment markedly impaired the leading edge stability of these cells (Figure S6). These results suggest that MLCK might play a conserved role in the regulation of neutrophil polarity and chemotaxis under different microenvironmental settings.

The specificity of ML-7 for MLCK, instead of for other protein kinase including protein kinase A (PKA), was demonstrated at a similar concentration³⁰. Nevertheless to further confirm the specificity of ML-7, we used RNAi-mediated knockdown to deplete MLCK in dHL-60 cells. Depletion of MLCK led to similar defects (Supplementary Text; Fig. S7A-S7D). In addition, consistent with their effects on the leading edges, MLCK inhibition and depletion prevented accumulation of polymerized actin, 3'-phosphoinositol lipids (PI3Ps) and Rac-GTP at the leading edge (Supplementary Text and Figure S7E and S8). Actin polymers, PI3Ps and Rac-GTP are key components of the "frontness" pathway and play essential roles in establishing the leading edge during neutrophil chemotaxis^{1,4}. Thus, our results show that MLCK is spatially recruited to the leading edge and is necessary for leading edge stability during neutrophil chemotaxis.

MRLCs are the only known substrate for MLCK²⁷. The asymmetric distribution of MLCK prompted us to ask whether this kinase would selectively control the activity of myosin II at the leading edge. The ratio of mean immunofluorescence intensity of p[19]-MRLC between the leading and the trailing

edge was ~25% lower in ML-7-treated dHL-60 cells than in the control cells (Figure 3D and 3E), suggesting that MLCK inhibition impaired the accumulation of activated myosin II at the leading edge compared with the rest of the cell body. The use of ratio of mean fluorescence intensity discounts the variations in the levels of fluorescence probes among cells and is thus more appropriate for assessing the relative accumulation of the fluorescent signals. Furthermore, treatment with the p160-ROCK inhibitor Y-27632 sharply reduced the distribution of phosphorylated myosin II at the trailing edge (Figure 3D), in keeping with an earlier report⁴. Inhibition of myosin II activity by ML-7 and Y-27632 was also demonstrated by western blotting of total p[19]-MRLC levels (Figure 3F). Intriguingly, both ML-7 and Y-27632 treatments increased the relative distribution of myosin IIA protein at the leading edge (Figure 3G; 24% and 41%, respectively), probably due to the alterations in overall cytoskeletal organization. Taking into account the increased distribution of myosin IIA at the front, we inferred that ML-7 caused >30% decrease in the relative level of activated myosin II (i.e., p[19]-MRLC/total myosin IIA) at the leading edge.

Inhibiting or depleting MLCK in neutrophils markedly reduced the tractions at the leading edge (Figure 4A, 4B; Supplementary Movie S12) in cells migrating on the substrate with 3.5 kPa of stiffness (Table 1). Interestingly, the same treatments also reduced the tractions at the trailing edge (Figure 4A, 4B) (Table 1). Furthermore, MLCK inhibition (or depletion) abolished the periodic pattern of tractions at both the leading and the trailing edge in dHL-60 cells and primary neutrophils (Figure 4B-4C, Figure S9A-9B and Figure S10A). Because the tractions in MLCK-inhibited/depleted cells were reduced at both edges and were no longer periodic, this finding suggested coordination and coupling of tractions at the front and the back under this matrix-stiffness condition. In keeping with this notion, treatment of cells with Y-27632 also substantially reduced the tractions and prevented the

periodic oscillations at both the leading and the trailing edge (Figure 4D-4F, Figure S9C and Figure S10B) (Table 1).

It was recently documented that the chemotactic behaviors of neutrophils were influenced by substrate stiffness¹². To investigate whether MLCK played a more conserved role in the regulation of tractions, we assessed the effect of MLCK inhibition in neutrophils migrating on a stiffer substrate (100 kPa). Primary neutrophils migrating towards a fMLP-containing micropipette exerted higher tractions under this condition, in keeping with the previous report¹² (Table 1). Traction at the leading and the trailing edge both demonstrated periodicity (4.7 ± 1.5 sec and 4.7 ± 1.3 sec, respectively) and were out of phase by 1.0 ± 0.3 sec (Figure 5A-5B). Myosin II inhibition, as expected, markedly reduced the levels and prevented the periodicity of traction at both edges (Figure S11A). MLCK inhibition exerted very similar effects on tractions to blebbistatin treatment (Fig. S11B). Intriguingly, although treatment of cells with Y-27632 reduced tractions by 40-45% (Table 1), the cells nevertheless exhibited periodic tractions at both edges (4.7 ± 0.9 sec and 5.0 ± 1.3 sec, respectively) (Figure 5C), with a lag of 0.90 ± 0.33 sec (Figure 5D). These results suggest a differential regulatory pattern of tractions in cells migrating on the stiffer substrate.

MLCK regulates leading edge adhesion by activating $\alpha 5 \beta 1$ -integrin

How does MLCK-mediated myosin contractility control leading-edge stability in neutrophils? During migration protrusion and adhesion of the leading edge are tightly coupled³¹. Cell adhesion sites are required to stabilize leading edges and promote cell polarity in cells migrating on flat surfaces³¹. MLCK-mediated myosin II contractility may be necessary for leading edge protrusion. Alternatively, the defects of MLCK inhibition (or depletion) on neutrophil polarity can be interpreted as the inability

of the cells to attach their protrusive pseudopods, resulting in unstable and poorly developed leading edges. Indeed, blocking leading edge adhesion of neutrophils with RGD peptides targeting $\alpha 5 \beta 1$ -integrin, the main fibronectin receptors in neutrophils, caused defects highly reminiscent of those induced by MLCK inhibition (Supplementary Text and Figure S12).

MLCK inhibition markedly impaired neutrophil adhesion. First, experiments with a commonly used cell plating assay demonstrated that MLCK inhibition compromised adhesion of dHL-60 cells to fibronectin (Figure 6A). Interestingly, MLCK inhibition specifically prevented cell adhesion induced by fMLP, because ML-7 had little effect on cell adhesion to fibronectin in the absence of fMLP stimulation (Figure 6A). To further analyze adhesion at the single cell level, we used total internal reflection fluorescence (TIRF) microscopy in dHL-60 cells expressing GFP-tagged $\alpha 5$ -integrin. The goal of this experiment was to assess whether MLCK inhibition impaired $\alpha 5 \beta 1$ -integrin-mediated leading edge attachment. The evanescent wave causes excitation of fluorescent molecules in an optical section (<100 nm) without exciting molecules throughout the specimen and allows visualization of signaling activity in living cells in contact with the coverglass (substrate). In response to a point source of fMLP gradient, neutrophils extended a protrusive leading edge and established contact with the fibronectin substrate, as indicated by the emergence of GFP fluorescence at the leading edge (Figure S13A). In addition, de-adhesion and retraction of trailing edge was apparent, as suggested by the disappearance of GFP fluorescence at the trailing edge of migrating cells (Figure S13A). MLCK inhibition markedly impaired leading edge attachment, as suggested by the absence or reduction of fluorescent signals of GFP- $\alpha 5$ integrin at the leading edge (Figure S13B). We analyzed attachment quantitatively in control and MLCK-inhibited cells by measuring TIRF signals within the leading edge (as defined by DIC images) (Figure 6B). This analysis suggested that MLCK inhibition reduced

leading edge adhesion by 78% (Figure 6B). In contrast, the same treatment only slightly altered attachment of the area outside the leading edge (denoted as Cell body) (Figure 6B: right panel). Thus, MLCK inhibition impaired leading edge adhesion. However, these results alone could not distinguish whether MLCK mediates leading edge protrusion or adhesion, as discussed above. As expected, cells treated with Y-27632 exhibited long stretched tail that failed to retract properly, while cells with blebbistatin treatment showed defects in both leading edge attachment and tail retraction (Figure S13C-13D).

We next asked whether MLCK was necessary for leading edge protrusion. We took advantage of a feature of neutrophils: their ability to polarize when stimulated with chemoattractants, even in suspension. When exposed to fMLP, neutrophils in suspension quickly (within 1–2 min) establish a morphological leading edge³². The leading edge does not persist and retracts after stimulation^{2,33-35}. Attractant stimulation of neutrophils in suspension also suffices to lead to accumulation of polymerized actin, PI3Ps and Rac-GTP, albeit transiently, consistent with the morphological response^{1,2,4}. When held with a pipette, dHL-60 cells responded to a gradient of fMLP from an adjacent pipette by extending a leading edge (Figure S14A). The leading edge continued to grow and then retracted. Cells treated with ML-7 exhibited no detectable defects in the protrusive behavior and dynamics when stimulated with the fMLP gradient (Figure S14A and S14B). We next measured the level of polymerized actin, Rac-GTP and phospho-Akt (activated Akt, readout for PI3Ps)^{2,4} with or without fMLP stimulation. Consistent with previous findings^{1,2,4}, fMLP addition induced a rapid and transient accumulation of polymerized actin, phospho-Akt and Rac-GTP in neutrophils in suspension, which peaked at 30–60 sec after stimulation (Figure S14C-S14E). Treatment with ML-7 failed to prevent any of these frontness markers in cells exposed to fMLP in suspension (Figure S14C-S14E). Therefore,

MLCK is not required for protrusion *per se* but appears to regulate leading edge adhesion. In addition, because MLCK inhibition/depletion impaired the leading edge accumulation of PI3Ps, Rac-GTP and actin polymers in adherent cells (Figure S7E and S8), these results imply that cell adhesion is necessary for the stability of the frontness signals.

Integrin activation refers to a switch from a low-affinity to a high-affinity state of ligand binding. Integrin activation is the key step for cell adhesion to the ECM³⁶. To explain how MLCK controls cell adhesion during neutrophil chemotaxis, we tested if MLCK is involved in integrin activation during chemotaxis. We assessed the localization and expression of activated $\alpha 5\beta 1$ -integrin with a GST-tagged protein containing the 9th to 11th fibronectin type III repeats (GST-FN III₉₋₁₁), which specifically binds active $\alpha 5\beta 1$ -integrin¹⁴. While total $\alpha 5\beta 1$ -integrin (as detected by anti- $\alpha 5$ -integrin antibody) was found evenly distributed throughout the cell, activated $\alpha 5\beta 1$ integrin was enriched at the leading edge of polarized dHL-60 cells [Figure 6C; A focal plane from the confocal microscopy analysis is shown]. Consistently, the line profile of the polarized cell exhibited highest level of GST-FN III₉₋₁₁ binding at the leading edge (Figure 6C). MLCK inhibition caused the level of active $\alpha 5\beta 1$ -integrin to markedly reduce at the leading edge, whereas the localization pattern of total $\alpha 5\beta 1$ -integrin remained unchanged (Figure 6D). Incubation of cells with GST alone failed to produce fluorescent signals (Figure S14F). These results suggest that MLCK controls $\alpha 5\beta 1$ -integrin activity at the neutrophil's leading edge.

We next assessed the level of activated $\alpha 5\beta 1$ -integrin in cells with or without MLCK inhibition biochemically. As shown in Figure 6E, ML-7 exerted little effect on fMLP-induced activation in neutrophils in suspension, indicating that MLCK activity is not necessary for the inside-out activation

of $\alpha 5\beta 1$ -integrin by fMLP (i.e., in the absence of adhesion to ECM). However, the same treatment prevented $\alpha 5\beta 1$ -integrin activation when cells were attached to the fibronectin substrate (Figure 6F), demonstrating that MLCK is necessary for $\alpha 5\beta 1$ -integrin activation in adherent cells. The dependence of MLCK-mediated integrin activity on cell-ECM adhesion suggested that tractions may play a special role in this regulation. Traction-induced cytoskeletal tension could activate integrin mechanically, as discussed later.

Discussion

Taken together, our results reveal novel mechanical aspects of cell polarity and motility in neutrophils and are summarized in a model (Figure 7). We discovered a periodic pattern of tractions at the leading and the trailing edge in a neutrophil-like cell line and primary neutrophils during chemotaxis. This oscillatory pattern has not been documented for any biochemical or mechanical factors in neutrophils during chemotaxis. What might be the function of the periodic tractions? We speculate that the oscillations at the front of the cell may be linked to the cycle of leading edge extension and adhesion. In this scenario, extension of the pseudopod occurs with minimal contact with the ECM substrate and is thus associated with weak tractions. In contrast, strong tractions could result from establishment and stabilization of leading edge attachment. In addition, the traction oscillations at the cell's rear may correspond to periodic contractions that enable the cell to pull the trailing edge forward. Interestingly, in addition to the periodic patterns, we found that the traction oscillations at the front and the back are out of phase, with the tractions at the front leading those at the back, thus pointing to a timing mechanism that allows neutrophils to coordinate leading edge adhesion and trailing edge de-adhesion to ensure persistent movements. We can only speculate about the molecular mechanism that gives rise to the temporal shift. Chemoattractant-induced activation of MLCK may precede that of p160-ROCK (Fig. 7), which could cause the delay in myosin II activation and myosin II contractility at the rear. This possibility could be tested by examining the temporal dynamics of MLCK, p160-ROCK and Rho activation in response to attractants, probably with high-sensitivity live cell biosensors for MLCK and p160-ROCK activities. Notably, our findings contrasted an earlier study in which traction stresses were detected mostly in the uropod of neutrophils migrating on a stiffer substrate (9 kPa)³⁷. The differential patterns of tractions observed may be attributed to the differences in substrate stiffness, temporal resolutions of the studies and/or other undefined factors.

How are tractions regulated in neutrophils during chemotaxis? Our current findings suggest that tractions at the leading and the trailing edge in neutrophils require myosin II activation. Inhibition of myosin II impairs the level and the periodicity of tractions. Our results suggest that the recruitment of MLCK to the neutrophil's leading edge activates MRLC and myosin II contractility, allowing cells to exert tractions on the ECM substrate, enhance integrin activity and stabilize leading edge adhesion (Figure 7). The spatially controlled activation of Rho, p160-ROCK and subsequent myosin II activation⁴ leads to contraction of actin-myosin complexes at the trailing edge, causing it to de-adhere (Figure 7). At least three possibilities, alone or in combination, could account for the periodic pattern of tractions. It might be that myosin II is activated periodically during chemotaxis. Alternatively, the strength of cell-substrate adhesion might be temporally regulated, leading to alternation of weak and strong local tractions during neutrophil migration. Third, there might be myosin II-independent mechanism(s) that might also contribute to the development and periodicity of tractions. In our experiments, there are significant amounts of tractions remaining after inhibition of total or localization-specific myosin II activities. Our results are in keeping with a recent report demonstrating that inhibition of myosin II functions fails to abolish tractions in *Dictyostelium* cells during chemotaxis³⁸. One group of putative candidates that might control tractions in neutrophils are plasma membrane-anchored myosin class I molecules, which reportedly could generate membrane tension by pulling on F-actin coupled to ECM via integrins³⁹. Other candidates include force-bearing cytoskeletal molecules such as microtubules and intermediate filaments that can transmit force to actin through various inter-cytoskeletal linkage^{40,41}. More complete understanding of the detailed mechanisms governing the periodic and out-of-phase behavior of tractions awaits future experiments. In addition, future experiments should investigate whether the observed spatiotemporal dynamics of tractions and its

regulatory pattern can be extended to neutrophils under other extracellular settings (e.g., on ECM substrates for β 2-integrin) and to other amoeboid cells.

In slow migrating cells such as fibroblasts, MLCK is mainly found in stress fibers ⁴². Distribution of MLCK in neutrophils differs from this pattern. As in neutrophils, MLCK and ROCK in fibroblasts play distinct roles in regulating membrane protrusions and adhesion dynamics during cell migration ⁴³. MLCK inhibition blocks MRLC phosphorylation at the cell periphery, but not in the center and prevent zyxin-containing adhesions at the periphery. These cells generate membrane protrusions all around the cell, turn more frequently, and migrate less effectively. In contrast, ROCK inhibition blocks MRLC phosphorylation in the center and prevents formation of focal adhesions. These cells move faster and straighter. Thus, although MRLC activation in fibroblasts is spatially controlled by MLCK and ROCK, their distribution and function in the control of cell migration seem to differ from neutrophils.

How might MLCK inhibition (or depletion) at the leading edge affect tractions at both edges in neutrophils during chemotaxis? It is well accepted that organization of actin cytoskeleton in cells is heavily dependent on mechanical force. Increasing tension in the actin network leads to formation of actin bundles, which can be prevented by the inhibition of myosin activity ^{44,45}. More recently, it was demonstrated that nonmuscle myosin II is required not only to establish but also to maintain integrity of the actomyosin network ⁴⁶. Based on these results, we speculate that the global effect of MLCK inhibition on tractions in neutrophils might be linked to its ability to regulate myosin II-dependent contractility. In this scenario, depletion or inhibition of MLCK impairs myosin II contractility at the leading edge and in turn disrupts the structure and organization of the actin cytoskeleton (Figure 7), as

shown by experiments with live and fixed neutrophils. Myosin II might crosslink actin filaments into a coherent mechanical network that allows transmission of force from one side of the cell to the other⁴⁴. In neutrophils, the actin cytoskeletal network appears highly organized and interconnected (Movie S4), and thus might provide a structural framework for the putative mechanotransduction activity. Alternatively, force might be transmitted through connections among different types of cytoskeletons, as shown in other cells and organisms^{41,47}. Thus, MLCK inhibition at the leading edge could also affect the structure and organization of the actin cytoskeleton at the trailing edge of the cells, leading to a decrease in tractions at the rear. Similarly, this model (Figure 7) also explains the decreased tractions at both edges of the cells after p160-ROCK is inhibited.

However, it is of note that the proposed model (Figure 7) cannot explain how p160-ROCK-inhibited neutrophils retain periodicity of tractions at both edges on stiffer substrate (100 kPa). It might be that a higher-stiffness substrate helps to better support and maintain cytoskeletal organization and integrity in neutrophils, rendering cells less susceptible to local inhibition of myosin II. Indeed, the degree of integrity and organization of actin cytoskeleton is closely related to mechanical properties of extracellular environment. More bundled, ordered stress fiber formation is observed in fibroblasts on stiffer matrix⁴⁸. Furthermore, p160-ROCK, unlike MLCK, is not required for leading edge activities and thus, when inhibited, exerts little effects on leading edge protrusion and stability. As such, the remaining myosin II activity after p160-ROCK inhibition could still enable the cells to maintain the pattern of tractions on both the leading and the trailing edge. An alternative possibility is that the putative myosin II-independent mechanism(s), as discussed earlier, might be actively engaged to support the periodic pattern of tractions at the back the cells under these conditions.

How does MLCK control integrin activation in neutrophils? Our results, as well as those from others, have begun to point to a role for myosin II-dependent mechanical tension. Friedland *et al.*⁴⁹ reported that $\alpha 5\beta 1$ -integrin can switch between relaxed and tensioned states in response to myosin II-generated cytoskeletal force. The resulting force combines with cell-substrate adhesion to generate tension that activates the integrin molecule mechanically. Our results also suggest that myosin II-dependent cellular contraction mediates the MLCK's effect on adhesion and integrin activation. MLCK inhibition fails to prevent integrin activation in neutrophils in suspension, implying the role of tractions in the regulation of integrin activity. We suspect that the tension applied to specific molecules (e.g., talin⁵⁰ or vinculin⁵¹) that control integrin activity might change their conformations to "active," as in the "conformational switch" model⁵² proposed to explain the maturation of focal adhesions by internal actin-myosin contraction in fibroblasts. In support of this notion, application of physiologically relevant forces causes stretching of single talin rods that expose cryptic binding sites for vinculin⁵³. Thus, the documented protein stretching may represent a more general mechanism for force transduction in a variety of signaling events including integrin activation.

Acknowledgements

We thank Dr. Anne Bresnick for providing the sMLCK-GFP construct, Dr. Rick Horwitz for providing EGFP- $\alpha 5$ integrin and mCherry-myosin IIA, and the members of the Wang lab for helpful discussion. This work was supported in part by NIH grants GM083812 (to F. Wang), GM083601 (to C. Rao and F. Wang), HD059002 (to D. Leckband and F. Wang), GM072744 (to N. Wang), the Illinois Regenerative Medicine Institute (IDPH 2006-05516; to F. Wang), NSF CAREER award 0953267 (to F. Wang) and the Arnold O. Beckman award from the University of Illinois (to F. Wang).

Author Contributions

MES, YH, DL, SN, FC, YCP, OC and PS performed research. FW and NW designed research. MAS and PL contributed vital reagents.

Conflict of Interest

The authors declare no conflict of interest.

References

1. Srinivasan S, Wang F, Glavas S, et al. Rac and Cdc42 play distinct roles in regulating PI(3,4,5)P3 and polarity during neutrophil chemotaxis. *J Cell Biol.* 2003;160:375-385.
2. Wang F, Herzmark P, Weiner OD, Srinivasan S, Servant G, Bourne HR. Lipid products of PI(3)Ks maintain persistent cell polarity and directed motility in neutrophils. *Nat Cell Biol.* 2002;4:513-518.
3. Wong K, Pertz O, Hahn K, Bourne H. Neutrophil polarization: spatiotemporal dynamics of RhoA activity support a self-organizing mechanism. *Proc Natl Acad Sci U S A.* 2006;103:3639-3644.
4. Xu J, Wang F, Van Keymeulen A, et al. Divergent signals and cytoskeletal assemblies regulate self-organizing polarity in neutrophils. *Cell.* 2003;114:201-214.
5. Rottner K, Hall A, Small JV. Interplay between Rac and Rho in the control of substrate contact dynamics. *Current Biology.* 1999;9:640-649.
6. Balaban NQ, Schwarz US, Riveline D, et al. Force and focal adhesion assembly: a close relationship studied using elastic micropatterned substrates. *Nat Cell Biol.* 2001;3:466-472.
7. Smith A, Carrasco YR, Stanley P, Kieffer N, Batista FD, Hogg N. A talin-dependent LFA-1 focal zone is formed by rapidly migrating T lymphocytes. *J Cell Biol.* 2005;170:141-151.
8. Servant G, Weiner OD, Herzmark P, et al. Polarization of Chemoattractant Receptor Signaling During Neutrophil Chemotaxis. *Science.* 2000;287:1037-1040.
9. Pelham RJ, Jr., Wang Y-l. High Resolution Detection of Mechanical Forces Exerted by Locomoting Fibroblasts on the Substrate. *Mol Biol Cell.* 1999;10:935-945.
10. Engler A, Bacakova L, Newman C, Hategan A, Griffin M, Discher D. Substrate Compliance versus Ligand Density in Cell on Gel Responses. *Biophys J.* 2004;86:617-628.

11. Tolic-Norrelykke IM, Butler JP, Chen J, Wang N. Spatial and temporal traction response in human airway smooth muscle cells. *Am J Physiol Cell Physiol*. 2002;283:C1254-1266.
12. Oakes PW, Patel DC, Morin NA, et al. Neutrophil morphology and migration are affected by substrate elasticity. *Blood*. 2009;114:1387-1395.
13. Manders EM, Stap J, Brakenhoff GJ, van Driel R, Aten JA. Dynamics of three-dimensional replication patterns during the S-phase, analysed by double labelling of DNA and confocal microscopy. *J Cell Sci*. 1992;103 (Pt 3):857-862.
14. Orr AW, Ginsberg MH, Shattil SJ, Deckmyn H, Schwartz MA. Matrix-specific Suppression of Integrin Activation in Shear Stress Signaling. *Mol Biol Cell*. 2006;17:4686-4697.
15. Eddy RJ, Pierini LM, Matsumura F, Maxfield FR. Ca²⁺-dependent myosin II activation is required for uropod retraction during neutrophil migration. *J Cell Sci*. 2000;113 (Pt 7):1287-1298.
16. Janmey PA, McCulloch CA. Cell mechanics: integrating cell responses to mechanical stimuli. *Annu Rev Biomed Eng*. 2007;9:1-34.
17. Bodin S, Welch MD. Plasma membrane organization is essential for balancing competing pseudopod- and uropod-promoting signals during neutrophil polarization and migration. *Mol Biol Cell*. 2005;16:5773-5783.
18. Gomez-Mouton C, Lacalle RA, Mira E, et al. Dynamic redistribution of raft domains as an organizing platform for signaling during cell chemotaxis. *J Cell Biol*. 2004;164:759-768.
19. Hauert AB, Martinelli S, Marone C, Niggli V. Differentiated HL-60 cells are a valid model system for the analysis of human neutrophil migration and chemotaxis. *Int J Biochem Cell Biol*. 2002;34:838-854.

20. Schymeinsky J, Sindrilaru A, Frommhold D, et al. The Vav binding site of the non-receptor tyrosine kinase Syk at Tyr 348 is critical for β_2 integrin (CD11/CD18)-mediated neutrophil migration. *Blood*. 2006.
21. Geiger B, Bershadsky A. Exploring the Neighborhood: Adhesion-Coupled Cell Mechanosensors. *Cell*. 2002;110:139-142.
22. Maupin P, Phillips CL, Adelstein RS, Pollard TD. Differential localization of myosin-II isozymes in human cultured cells and blood cells. *J Cell Sci*. 1994;107:3077-3090.
23. Vicente-Manzanares M, Zareno J, Whitmore L, Choi CK, Horwitz AF. Regulation of protrusion, adhesion dynamics, and polarity by myosins IIA and IIB in migrating cells. *J Cell Biol*. 2007;176:573-580.
24. Weiner OD, Rentel MC, Ott A, et al. Hem-1 complexes are essential for Rac activation, actin polymerization, and myosin regulation during neutrophil chemotaxis. *PLoS Biol*. 2006;4:e38.
25. Pestonjamasp KN, Forster C, Sun C, et al. Rac1 links leading edge and uropod events through Rho and myosin activation during chemotaxis. *Blood*. 2006;108:2814-2820.
26. Alblas J, Ulfman L, Hordijk P, Koenderman L. Activation of RhoA and ROCK are essential for detachment of migrating leukocytes. *Mol Biol Cell*. 2001;12:2137-2145.
27. Kamm KE, Stull JT. Dedicated myosin light chain kinases with diverse cellular functions. *J Biol Chem*. 2001;276:4527-4530.
28. Wilson AK, Gorgas G, Claypool WD, de Lanerolle P. An increase or a decrease in myosin II phosphorylation inhibits macrophage motility. *J Cell Biol*. 1991;114:277-283.
29. Klemke RL, Cai S, Giannini AL, Gallagher PJ, de Lanerolle P, Cheresch DA. Regulation of cell motility by mitogen-activated protein kinase. *J Cell Biol*. 1997;137:481-492.

30. Bain J, McLauchlan H, Elliott M, Cohen P. The specificities of protein kinase inhibitors: an update. *Biochem J.* 2003;371:199-204.
31. Ridley AJ, Schwartz MA, Burridge K, et al. Cell migration: integrating signals from front to back. *Science.* 2003;302:1704-1709.
32. Zhelev DV, Alteraifi AM, Chodniewicz D. Controlled pseudopod extension of human neutrophils stimulated with different chemoattractants. *Biophys J.* 2004;87:688-695.
33. Fechheimer M, Zigmond SH. Changes in cytoskeletal proteins of polymorphonuclear leukocytes induced by chemotactic peptides. *Cell Motil.* 1983;3:349-361.
34. Sklar LA, Omann GM, Painter RG. Relationship of actin polymerization and depolymerization to light scattering in human neutrophils: dependence on receptor occupancy and intracellular Ca^{++} . *J Cell Biol.* 1985;101:1161-1166.
35. Ydrenius L, Molony L, Ng-Sikorski J, Andersson T. Dual action of cAMP-dependent protein kinase on granulocyte movement. *Biochem Biophys Res Commun.* 1997;235:445-450.
36. Hynes RO. Integrins: bidirectional, allosteric signaling machines. *Cell.* 2002;110:673-687.
37. Smith LA, Aranda-Espinoza H, Haun JB, Dembo M, Hammer DA. Neutrophil traction stresses are concentrated in the uropod during migration. *Biophys J.* 2007;92:L58-60.
38. Meili R, Alonso-Latorre B, del Alamo JC, Firtel RA, Lasheras JC. Myosin II is essential for the spatiotemporal organization of traction forces during cell motility. *Mol Biol Cell;*21:405-417.
39. Nambiar R, McConnell RE, Tyska MJ. Control of cell membrane tension by myosin-I. *Proc Natl Acad Sci U S A.* 2009;106:11972-11977.
40. Wang N, Tytell JD, Ingber DE. Mechanotransduction at a distance: mechanically coupling the extracellular matrix with the nucleus. *Nat Rev Mol Cell Biol.* 2009;10:75-82.

41. Rodriguez OC, Schaefer AW, Mandato CA, Forscher P, Bement WM, Waterman-Storer CM. Conserved microtubule-actin interactions in cell movement and morphogenesis. *Nat Cell Biol.* 2003;5:599-609.
42. Katoh K, Kano Y, Amano M, Kaibuchi K, Fujiwara K. Stress fiber organization regulated by MLCK and Rho-kinase in cultured human fibroblasts. *Am J Physiol Cell Physiol.* 2001;280:C1669-1679.
43. Totsukawa G, Wu Y, Sasaki Y, et al. Distinct roles of MLCK and ROCK in the regulation of membrane protrusions and focal adhesion dynamics during cell migration of fibroblasts. *J Cell Biol.* 2004;164:427-439.
44. Sims JR, Karp S, Ingber DE. Altering the cellular mechanical force balance results in integrated changes in cell, cytoskeletal and nuclear shape. *J Cell Sci.* 1992;103 (Pt 4):1215-1222.
45. Amano M, Chihara K, Kimura K, et al. Formation of actin stress fibers and focal adhesions enhanced by Rho-kinase. *Science.* 1997;275:1308-1311.
46. Cai Y, Rossier O, Gauthier NC, et al. Cytoskeletal coherence requires myosin-IIA contractility. *J Cell Sci.* 2003;116:413-423.
47. Petrasek J, Schwarzerova K. Actin and microtubule cytoskeleton interactions. *Curr Opin Plant Biol.* 2009;12:728-734.
48. Yeung T, Georges PC, Flanagan LA, et al. Effects of substrate stiffness on cell morphology, cytoskeletal structure, and adhesion. *Cell Motil Cytoskeleton.* 2005;60:24-34.
49. Friedland JC, Lee MH, Boettiger D. Mechanically activated integrin switch controls alpha5beta1 function. *Science.* 2009;323:642-644.
50. Tadokoro S, Shattil SJ, Eto K, et al. Talin binding to integrin beta tails: a final common step in integrin activation. *Science.* 2003;302:103-106.

51. Critchley DR, Gingras AR. Talin at a glance. *J Cell Sci.* 2008;121:1345-1347.
52. Geiger B, Bershadsky A. Assembly and mechanosensory function of focal contacts. *Current Opinion in Cell Biology.* 2001;13:584-592.
53. del Rio A, Perez-Jimenez R, Liu R, Roca-Cusachs P, Fernandez JM, Sheetz MP. Stretching single talin rod molecules activates vinculin binding. *Science.* 2009;323:638-641.

Table 1. Magnitude of tractions in migrating neutrophils

	Front	Back
	(Pascal)	
dHL-60 cells (3.5 kPa)		
Control	180 ± 39	207 ± 27
ML-7	111 ± 26	118 ± 30
MLCK KD	110 ± 16	145 ± 54
Blebbistatin	136 ± 19	112 ± 14
Y 27632	99 ± 16	87 ± 18
1⁰ neutrophils (3.5 kPa)		
Control	56 ± 17	85 ± 30
ML-7	40 ± 5	55 ± 7
Blebbistatin	33 ± 6	56 ± 11
Y 27632	33 ± 8	27 ± 3
1⁰ neutrophils (100 kPa)		
Control	596 ± 93	638 ± 102
ML-7	399 ± 87	375 ± 37
Blebbistatin	310 ± 88	390 ± 67
Y 27632	361 ± 83	349 ± 49

Figure Legends

Figure 1. Spatiotemporal dynamics of tractions during neutrophil chemotaxis

(A) dHL-60 cells were allowed to migrate toward chemoattractant-containing micropipette (fMLP, 10 μ M) on a fibronectin-coated elastic polyacrylamide gel for the times indicated. The speed for cell migration is ~ 2.0 μ m/min, lower than the speed of cells on fibronectin-coated glass (~ 2.4 μ m/min). The cells also exhibit normal tail retraction on the elastic gel (data not shown). Traction maps of the cell are shown. Pseudocolor bar representing tractions is given in Pascal (Pa). Scale bar, 5 μ m. Arrow indicates the direction of fMLP gradient. The leading edge of a polarized neutrophil was defined as the area within the first 3 μ m of the cell (marked by a white line), while the rest of the cell was defined as the trailing edge (see Materials and Methods). The image series shows part (7.2 sec, for which the cell traveled ~ 0.24 μ m) of the whole migratory response. The movie of the cell in (A) is available in Supplementary Information. (B) Time series of traction maps from (A) (with three additional time points) was analyzed by a customized MATLAB program to determine the average tractions in both leading (front) and trailing edge (back) of the cells in a time-dependent manner. The graph shows part (~ 9 sec) of the whole migratory response. x axis indicates time in sec. y axis is in Pascal (Pa). The mean levels of tractions at the leading and the trailing edge were comparable. A graph of another cell with a longer migratory response is shown in Figure S1A. (C) PSD plots of tractions at the leading (left panel) and the trailing edge (right panel) of a migratory dHL-60 cell. PSD plots were generated based on the results from Fourier analysis of the traction values. y axis represents the power spectral density normalized to the highest peak value (=1). x axis shows the oscillation frequency (Hz) (top) or period (s) (bottom). 9 cells were analyzed, and a representative cell is shown. PSD plots of tractions in three cells combined are shown in Fig. S1B. (D) PSD plots of tractions at the leading (left panel) and the trailing edge (right panel) of a migratory primary neutrophil. 6 cells were analyzed, and data from

a representative cell is shown (**E**) Left panel: Cross correlation between tractions at the leading and the trailing edge against time offset during migration for individual dHL-60 cells. Dotted lines indicate zero offset. Note that the back traction lags the front as indicated by the maximum cross correlation at time offset of 0.8 sec. Data from 3 representative cells are shown. Time bar = 24 s. Right panel: Summary of time offsets between leading edges and trailing edges (n=9 cells) in dHL-60 cells. (**F**) Left panel: Cross correlation between tractions at the leading and the trailing edge against time offset during migration for individual primary neutrophils. Data from 2 representative cells are shown. Right panel: Summary of time offsets between leading edges and trailing edges (n=6 cells) in primary neutrophils.

Figure 2. Myosin II controls tractions and is necessary for neutrophil chemotaxis

(**A**) dHL-60 cells were stimulated for 3 min by a uniform concentration of 1 μ M fMLP. Cells were fixed with 3.7 % paraformaldehyde and stained with a specific anti-myosin heavy chain IIA (MHCIIA) antibody, anti-p[Ser19]MRLC antibody, and rhodamine-conjugated phalloidin to localize filamentous actin (F-actin). The corresponding DIC image is also shown. Scale bar, 10 μ m. (**B**) dHL-60 cells were transfected with mCherry-myosin IIA (mChe-myoIIA) and stimulated by a micropipette containing 10 μ M fMLP for the indicated times. mCherry-myosin IIA fluorescence and the corresponding DIC images are shown. Arrows point to the locations of myosin IIA at the leading and trailing edge. Scale bar, 10 μ m. The movie of the cell in (**B**) is available in Supplementary Information. (**C**) dHL-60 cells pretreated with blebbistatin (100 μ M, 30 min) were allowed to migrate toward chemoattractant-containing micropipette (fMLP, 10 μ M) on a fibronectin-coated elastic polyacrylamide gel for the indicated times. Cells treated with blebbistatin migrated at 1.0 μ m/min on the elastic gel. Traction maps of the cell are shown. Pseudocolor bar representing traction force is given in Pascal (Pa). Scale

bar, 10 μm . The leading edge (within the first 2.2 μm of the cell) is marked by a white line (see Materials and Methods). The image series shows part (5.6 sec) of the whole migratory response. **(D)** Time series of traction maps from **(C)** (with four additional time points) was analyzed by a customized MATLAB program to determine the average tractions in both leading (front) and trailing edges (back) of the cells in a time-dependent manner. The graph shows part (~ 9.6 sec) of the whole migratory response. x axis indicates time in sec. y axis is in Pascal (Pa). **(E)** PSD plots of tractions at the leading (left panel) and the trailing edge (right panel) of a migratory cell pretreated with blebbistatin (100 μM , 30 min). The whole migratory response was analyzed. y axis represents the power spectral density normalized to the highest peak value (=1). x axis shows the oscillation frequency (Hz) (top) or period (s) (bottom). Cells with myosin IIA depleted exhibited similar response (not shown). 10 cells were analyzed, and a representative cell is shown. Additional plots are shown in Fig. S2C. **(F)** Before exposure to attractant supplied by a micropipette containing 10 μM fMLP, cells were not pretreated (control), were pretreated with blebbistatin (Blebbis, 100 μM , 30 min), were infected with lentivirus containing myosin IIA-targeting shRNAs (MyoII KD), or were pretreated with Y-27632 (30 μM , 30 min). The three images in each row show the positions of individual cells (each identified with a superimposed letter) after the indicated times of exposure to fMLP. White and black arrows point to the poorly-developed leading edges and long stretched tails, respectively. Cells infected with virus containing a scramble shRNA exhibited similar response to uninfected control cells. Lower doses of blebbistatin (≤ 50 μM) were tested, which required prolonged period of incubation to exert the same effects as 100 μM blebbistatin (data not shown). Scale bar, 10 μm . Movies of cells with or without treatments are available in Supplementary Information. **(G)** DIC kymographs of a dHL-60 cell untreated or treated with inhibitors or myosin IIA shRNAs migrating toward an fMLP (10 μM)-containing micropipette. The left panel shows a portion of the neutrophils' leading edge under various

conditions. The dotted rectangles indicate the regions of the cell used to generate the kymographs (prior to fMLP stimulation). The actual lengths of the rectangles are 20 μm in the direction of the arrow. White scale bar = 1 μm . The right panel shows the DIC kymographs. White scale bar = 5 μm . In both panels white arrows indicate the direction of protrusion. Cells a, d, f and h in (F) were used for the analysis. ~8 min of migration was recorded.

Figure 3. MLCK inhibition/depletion impairs myosin II activity at the leading edge

(A) dHL-60 cells plated on fibronectin-coated coverslips were stimulated for 2 min with 1 μM fMLP, fixed with 3.7 % paraformaldehyde and stained with a specific anti-MLCK antibody (red) and Alexa fluor 488-conjugated phalloidin (green). The polarized distribution of endogenous MLCK was observed in 188 out of 269 polarized cells. (B) A dHL-60 cell treated with ML-7 (25 μM , 30 min) was exposed to a point source of 10 μM fMLP for the times indicated (bottom panel). The cell fails to migrate to the micropipette and shows poorly developed pseudopod (white arrow). An untreated dHL-60 cell (top panel) with well-developed, stable pseudopod is shown. Scale bars, 10 μm . (C) DIC kymographs (left) of a dHL-60, untreated or treated with ML-7, migrating toward an fMLP (10 μM)-containing micropipette. The dotted rectangles indicate the regions of the cell used to generate the kymographs (prior to fMLP stimulation). The actual lengths of the rectangles are 20 μm in the direction of the arrow. Left panel: scale bar = 1 μm . Right panel: scale bars = 5 μm . Arrows indicate the direction of protrusion. 5 min of migration was recorded. The speed of leading-edge protrusion was calculated based on the kymographs (right). The values are means \pm SEM ($n = 34$ for control, and 32 for cells treated with ML-7). Asterisks indicate that the value for cells with ML-7 treatment differs from the corresponding control by $P < 0.0001$. (D) dHL-60 cells not pretreated or pretreated with ML-7 (25 μM , 30 min) or Y-27632 (30 μM , 30 min) were stimulated for 3 min by a uniform concentration

of 1 μ M fMLP. Cells were fixed with 3.7 % paraformaldehyde and stained with the anti-MHCIIA antibody, anti-p[Ser19]MRLC antibody, and rhodamine-conjugated phalloidin. The corresponding DIC images are also shown. Scale bar, 10 μ m. **(E)** The distribution of p[Ser19]MRLC in dHL-60 cells with or without ML-7 treatment was analyzed. The mean fluorescence of p[Ser19]MRLC staining at the leading and the trailing edge of cells was determined using Image J software, and the ratios between the leading and the trailing edge (i.e., mean fluorescence intensity at the leading edge/mean fluorescence intensity at the trailing edge) are shown. Values were normalized to the ratio (=100%) in control cells and are means \pm SEM (n = 40 for control, and 30 for cells treated with ML-7). Student t tests compared data between experimental groups. Results significantly different from those of control are indicated by asterisks (*; p < 0.001). **(F)** Western blot of p[Ser19]MRLC. dHL-60 Cells were pretreated with no inhibitors, ML-7 (25 μ M, 30 min), or Y-276322 (30 μ M, 30 min) before exposure to fMLP for 2 min in suspension. A typical blot is shown (top panel). The bottom panel shows quantification of blots from four separate experiments. Each bar represents the mean \pm SEM (error bars). All values were normalized to the signal (=100%) detected without the inhibitors. Asterisks indicate that the value for cells treated with M-7 or Y-27632 differs statistically from the control (*, p<0.01; **, p<0.001). Total MHCIIA levels were unaltered with the treatments and was used for equal loading in the different lanes. **(G)** The distribution of total MHCIIA in control dHL-60 cells and cells pretreated with ML-7 or Y-27632 was analyzed. The mean fluorescence of MHCIIA staining at leading and trailing edges was assessed by Image J software, and the ratios between leading and trailing edges are shown. Values were normalized to the ratio (=100%) in control cells and are means \pm SEM (n = 40 for control, 30 for cells treated with ML-7, and 25 for cells treated with Y-27632). Results significantly different from those of control are indicated by asterisks (*, p < 0.05; **, p < 0.001).

Figure 4. Localization-specific myosin activities are necessary for tractions in neutrophils

(A) dHL-60 cells with MLCK depleted were allowed to migrate toward chemoattractant-containing micropipette (fMLP, 10 μ M) on a fibronectin-coated elastic polyacrylamide gel for the indicated times. Traction maps of the cell are shown. Pseudocolor bar representing tractions is given in Pascal (Pa). Scale bar, 5 μ m. The leading edge (within the first 2.2 μ m of the cell) is marked by a white line. The image series shows part (5.6 sec) of the whole migratory response. Cells treated with ML-7 exhibited similar responses. Cells treated with ML-7 or with MLCK depleted migrated at 1.1 μ m/min on the elastic gel. The movie of the cell in (A) is available in Supplementary Information. (B) Time series of traction maps from (A) (with five additional time points) was analyzed by a customized MATLAB program to determine the average traction force in both leading (front) and trailing edges (back) of the cells in a time-dependent manner. The graph shows part (~9.6 sec) of the whole migratory response. x axis indicates time in sec. y axis is in Pascal (Pa). (C) PSD plots of tractions at the leading (left panel) and the trailing edge (right panel) of a migratory cell with MLCK depleted. The whole migratory response was analyzed. y axis represents the power spectral density normalized to the highest peak value (=1). x axis shows the oscillation frequency (Hz) (top) or period (s) (bottom). Cells pretreated with ML-7 exhibited similar response (not shown). 10 cells were analyzed, and a representative cell is shown. Additional plots for ML-7 treatment and MLCK depletion are shown in Figure S9A and Figure S9B. (D) dHL-60 cells pretreated with Y-27632 (30 μ M, 30 min) were allowed to migrate toward chemoattractant-containing micropipette (fMLP, 10 μ M) on a fibronectin-coated elastic polyacrylamide gel for the indicated times. Traction force maps of the cell are shown. Pseudocolor bar representing traction force is given in Pascal (Pa). Scale bar = 10 μ m. The leading edge (within the first 3 μ m of the cell) is marked by a white line (see Materials and Methods). The image series shows part (5.6 sec) of the whole migratory response. (E) Time series of traction maps from (D) (with five

additional time points) was analyzed by a customized MATLAB program to determine the average traction force in both leading (front) and trailing edges (back) of the cells in a time-dependent manner. The graph shows part (~9.6 sec) of the whole migratory response. x axis indicates time in sec. y axis is in Pascal (Pa). **(F)** PSD plots of tractions at the leading (left panel) and the trailing edge (right panel) of a migratory cell pretreated with Y-27632. The whole migratory response was analyzed. y axis represents the power spectral density normalized to the highest peak value (=1). x axis shows the oscillation frequency (Hz) (top) or period (s) (bottom). 8 cells were analyzed, and a representative cell is shown. Additional plots are shown in Fig. S9C.

Figure 5. The pattern and regulation of tractions in neutrophils migrating on a stiffer substrate

(A) PSD plots of tractions at the leading (left panel) and the trailing edge (right panel) of a migratory primary neutrophil. PSD plots were generated based on the results from Fourier analysis of the traction values. y axis represents the power spectral density normalized to the highest peak value (=1). x axis shows the oscillation frequency (Hz) (top) or period (s) (bottom). Primary cells were allowed to migrate toward chemoattractant-containing micropipette (fMLP, 10 μ M) on a fibronectin-coated polyacrylamide gel (100 kPa) for 4-5 min. 6 cells were analyzed, and a representative cell is shown. **(B)** Left panel: Cross correlation between tractions at the leading and the trailing edge against time offset during migration for individual primary neutrophils. Dotted lines indicate zero offset. Data from 3 representative cells are shown. Time bar = 24 s. Right panel: Summary of time offsets between leading edges and trailing edges (n=6 cells) in primary cells. **(C)** PSD plots of tractions at the leading (left panel) and the trailing edge (right panel) of a migratory primary neutrophil pretreated with Y-27632 (30 μ M, 30 min). PSD plots were generated based on the results from Fourier analysis of the traction values. y axis represents the power spectral density normalized to the highest peak value (=1). x axis

shows the oscillation frequency (Hz) (top) or period (s) (bottom). Cells were allowed to migrate toward chemoattractant-containing micropipette (fMLP, 10 μ M) on a fibronectin-coated polyacrylamide gel (100 kPa) for 4-5 min. 6 cells were analyzed, and a representative cell is shown. **(D)** Left panel: Cross correlation between tractions at the leading and the trailing edge against time offset during migration for individual Y-27632-treated primary neutrophils. Dotted lines indicate zero offset. Data from 3 representative cells are shown. Time bar = 24 s. Right panel: Summary of time offsets between leading edges and trailing edges (n=6 cells) in Y-27632-treated primary cells.

Figure 6. MLCK controls neutrophil adhesion and integrin activation

(A) dHL-60 cells pretreated with (25 μ M, 30 min) or without ML-7 were not stimulated or stimulated in suspension by 1 μ M fMLP and allowed to adhere to fibronectin-coated surface for 30 min, after which the degree of cell adhesion was assessed. Values were normalized to adhesion in control cells (=100%) with fMLP and are means \pm SEM (n=4). Results significantly different from those of control are indicated by asterisks (*, $p < 0.001$). **(B)** Assessment of adhesion area in leading edge and cell body in control and ML-7-treated cells transfected with EGFP- α 5-integrin and exposed to a point source of 10 μ M fMLP. Cell images were from Figure S13. Left panel: The time point at which leading edge protrusion of individual cell's was maximal was selected for analysis. Leading edge (denoted as "L") in TIRF image was demarcated by the corresponding DIC image, and the rest of the cell was defined as Cell body (denoted as "C"). Right panel: fluorescence intensities of the leading edge and the cell body in the TIRF images of control and ML-7-treated cells were determined with Image J, and the resulting values were used to quantify cell attachment of the both leading edge and the cell body. The plot shows the relative values in each region compared to control (=100%) in the presence of fMLP stimulation. Values are means \pm SEM (n=13 for control, 11 for cells treated with

ML-7). Results significantly different from those of control are indicated by asterisks (*; $p < 0.0001$).

(C, D) Upper panel: Localization of activated $\alpha 5\beta 1$ integrins in polarized neutrophils pretreated with or without ML-7 (25 μM , 30 min). dHL-60 cells pretreated with or without ML-7 were plated on fibronectin-coated coverslips and stimulated for 3 min by 1 μM fMLP. After washing, cells were fixed with 3.7 % paraformaldehyde, incubated with GST-FN III₉₋₁₁ (50 $\mu\text{g/ml}$) for 15 min at 37°C, and stained with an anti-GST antibody and anti- $\alpha 5$ -integrin antibody. Fluorescent and phase contrast images were collected by using confocal fluorescence microscopy. The images of a representative cell for each condition are shown (n=20 for control and n=17 for ML-7 treatment). Arrows indicate the leading edge. White line indicates the path along which line profile was obtained. The weak signals for GST-FN binding may be attributed to the relative low levels of activated $\alpha 5\beta 1$ -integrin in the cells. Scale bar, 10 μm . Lower panel: Line profiles of GST-FN III₉₋₁₁ and $\alpha 5$ -integrin fluorescence in cells shown in the upper panel. The graphs plot fluorescence intensity of each protein (y axis; in arbitrary unit) versus distance (x axis in pixels) along the white line on the phase contrast image of the cells. (E, F) Levels of activated $\alpha 5\beta 1$ integrins in cells with or without ML-7 treatment. dHL-60 cells pretreated with or without ML-7 were stimulated by a uniform concentration of fMLP (1 μM) in either suspension (E) or adhesion conditions (F). A typical blot is shown on the left. The right panel shows quantification of blots from four separate experiments. The y axis represents relative intensities (measured with Image J) with values normalized to the signal (=1) detected in the control cells without ML-7 treatment. Each bar represents the means \pm SEM (n=4). Results significantly different from those of cells without fMLP stimulation are indicated by asterisks (*, $p < 0.0001$; **, $p < 0.001$)

Figure 7. Integration of mechanical and biochemical signals to regulate leading edge adhesion and trailing edge de-adhesion: A model.

The model is proposed based on analyses of cell migration on the 3.5 kPa substrate. See text for details.

GPCR: G protein-coupled receptor

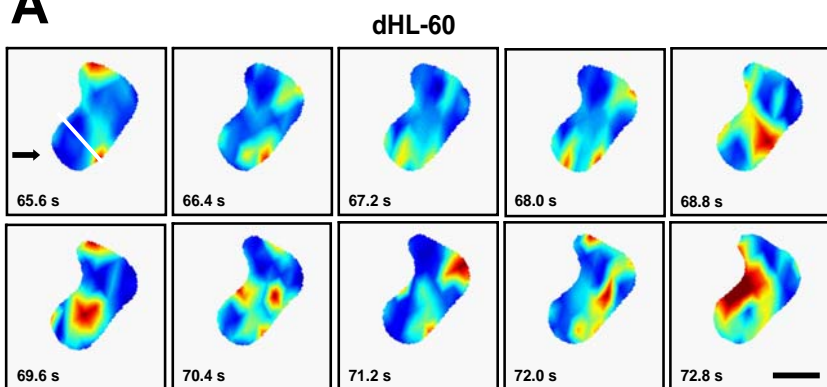
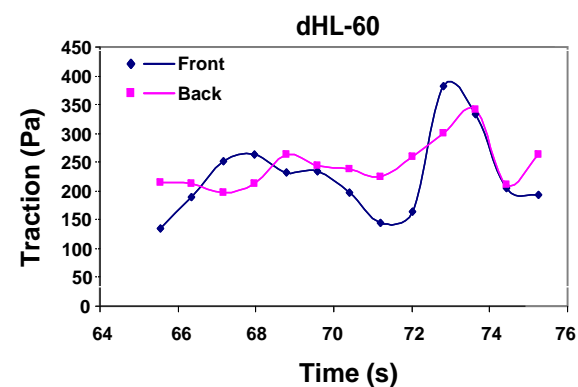
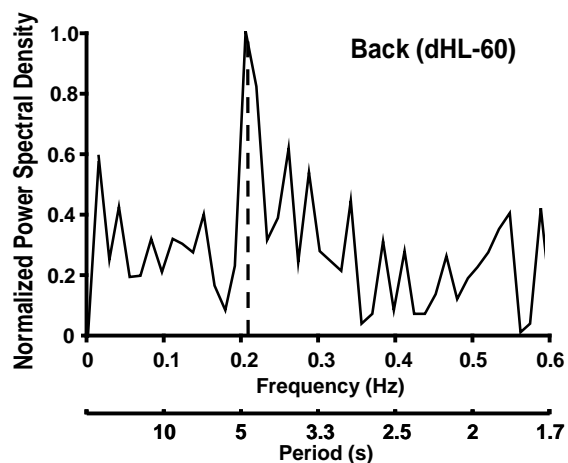
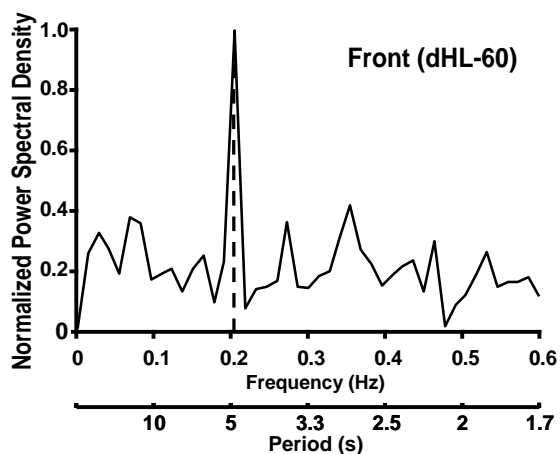
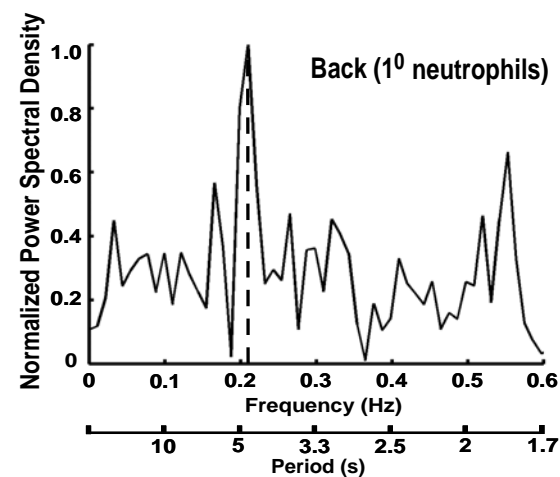
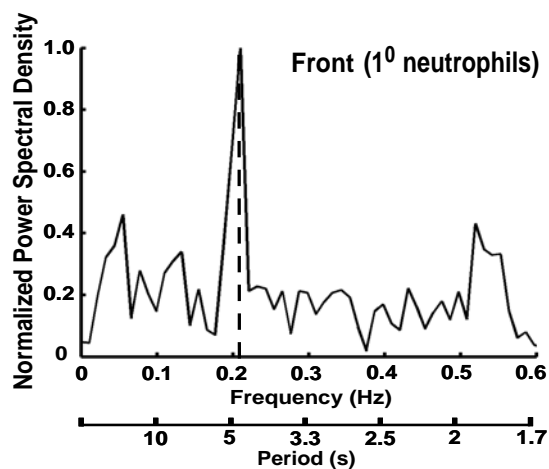
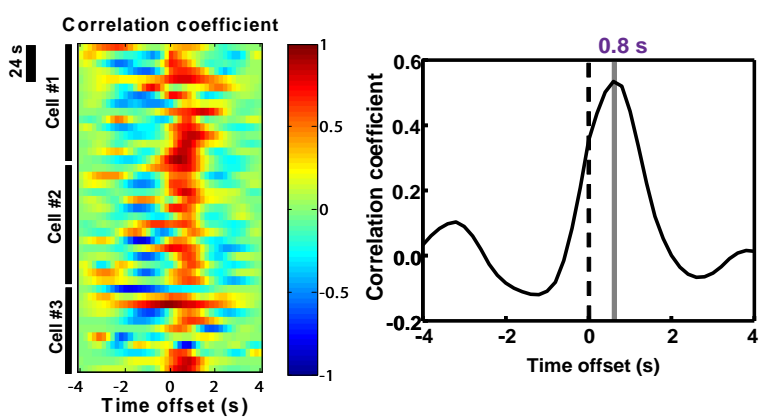
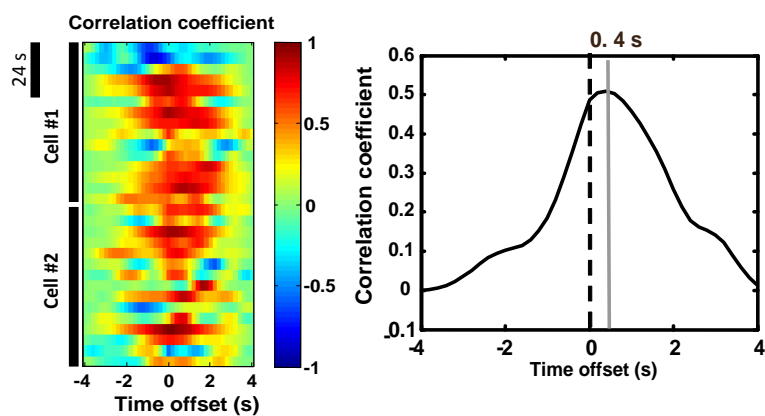
A**B****C****D****E****F**

Figure 1

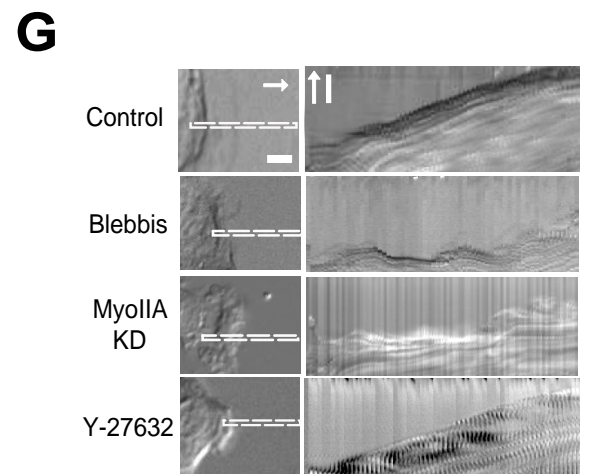
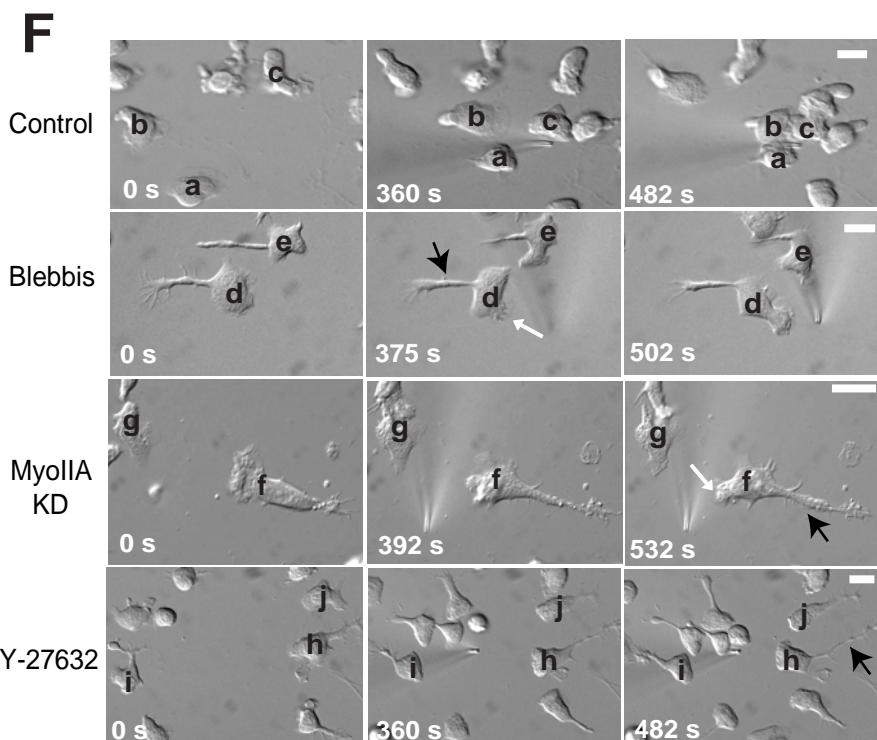
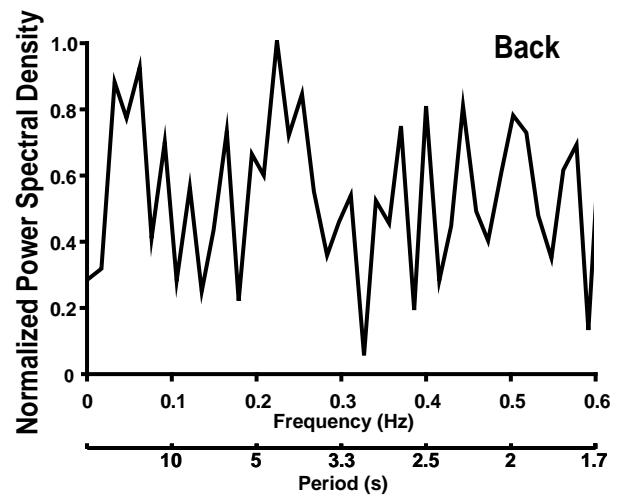
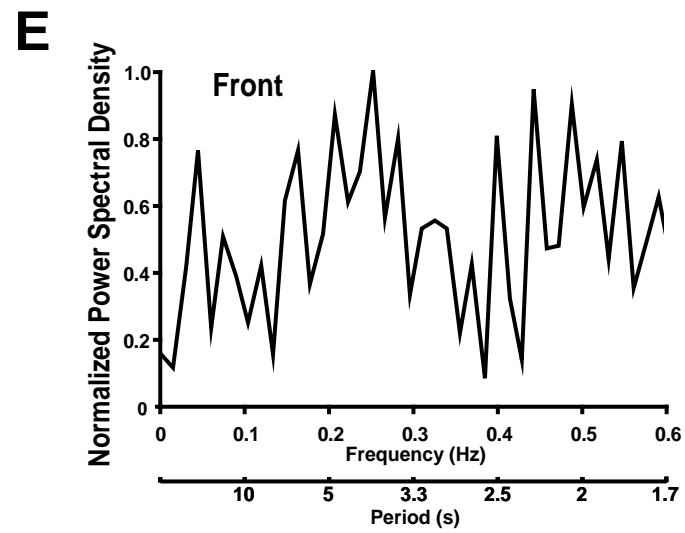
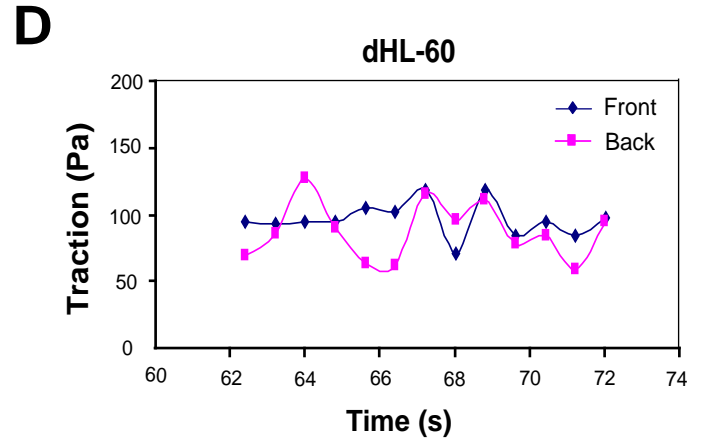
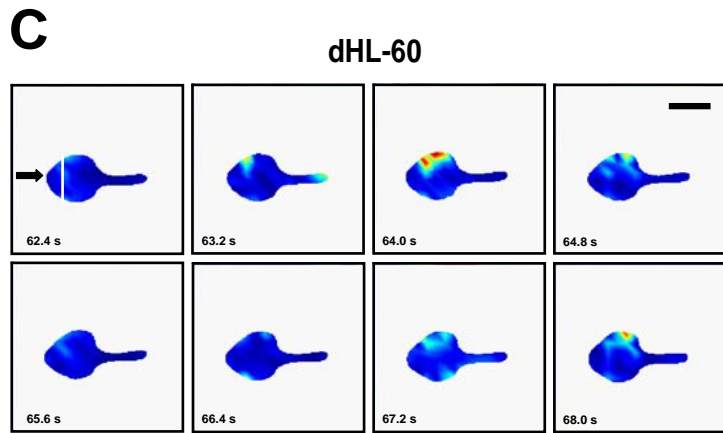
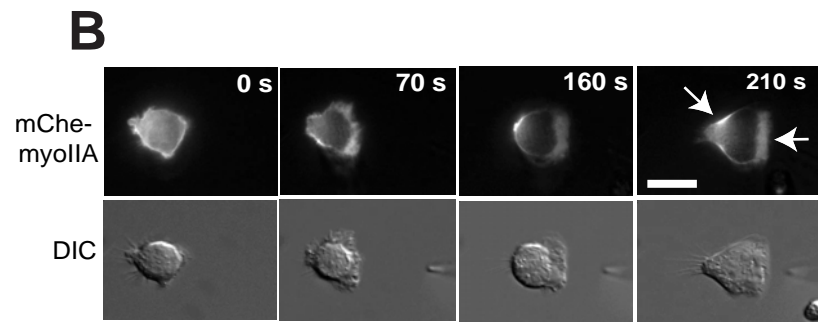
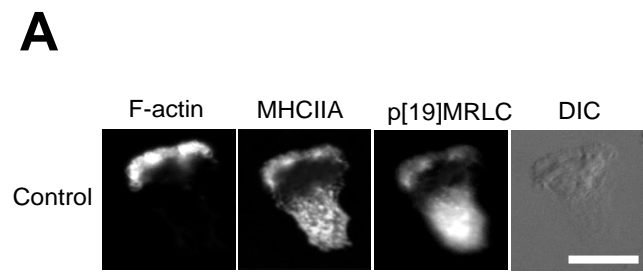


Figure 2

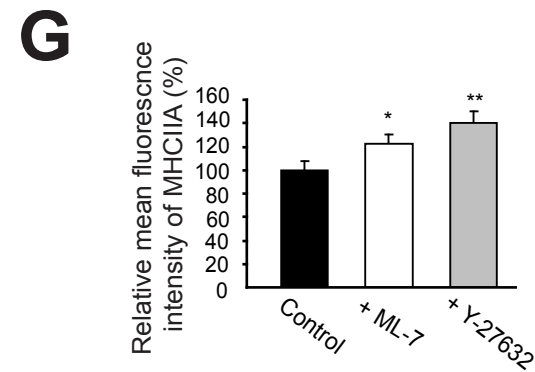
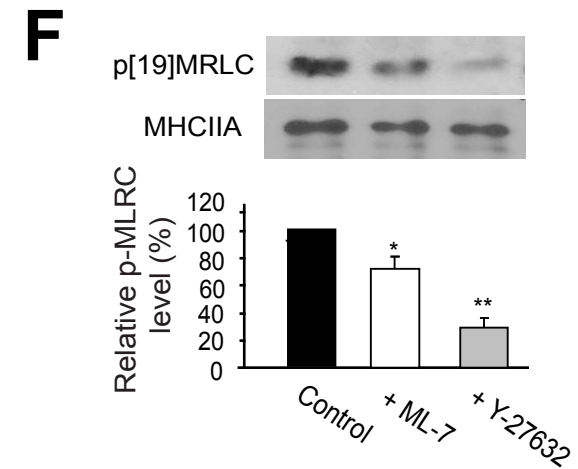
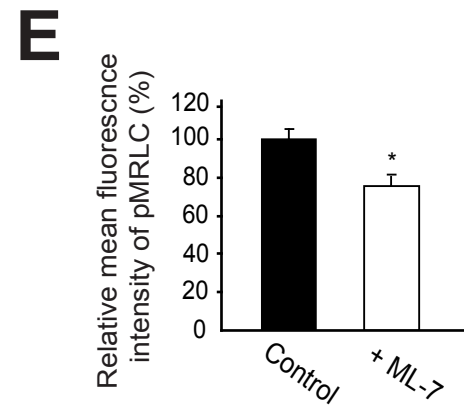
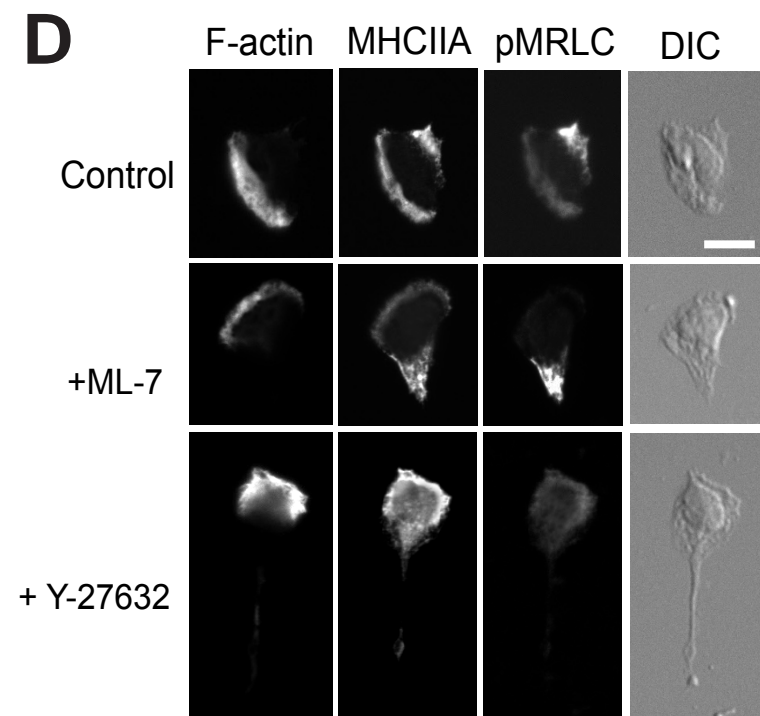
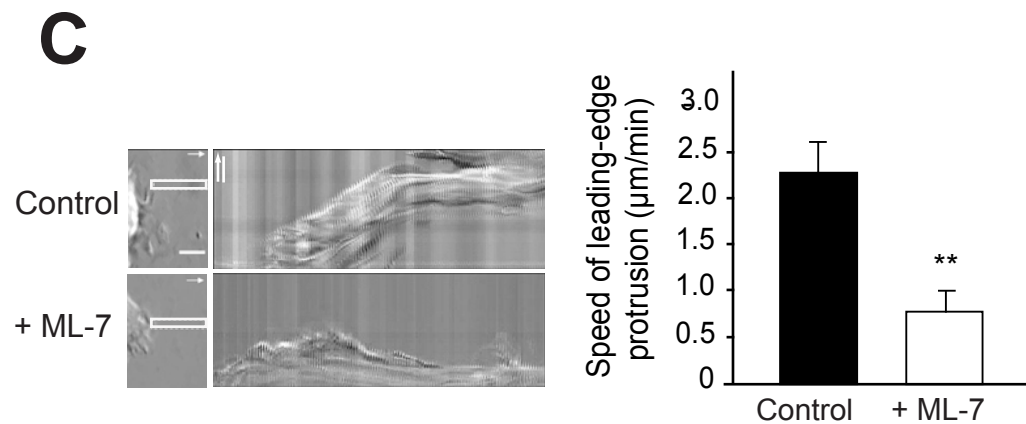
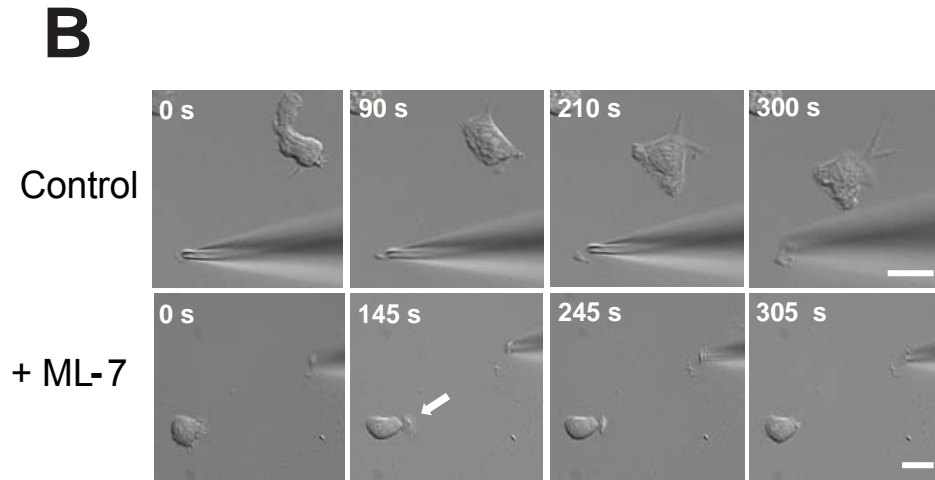
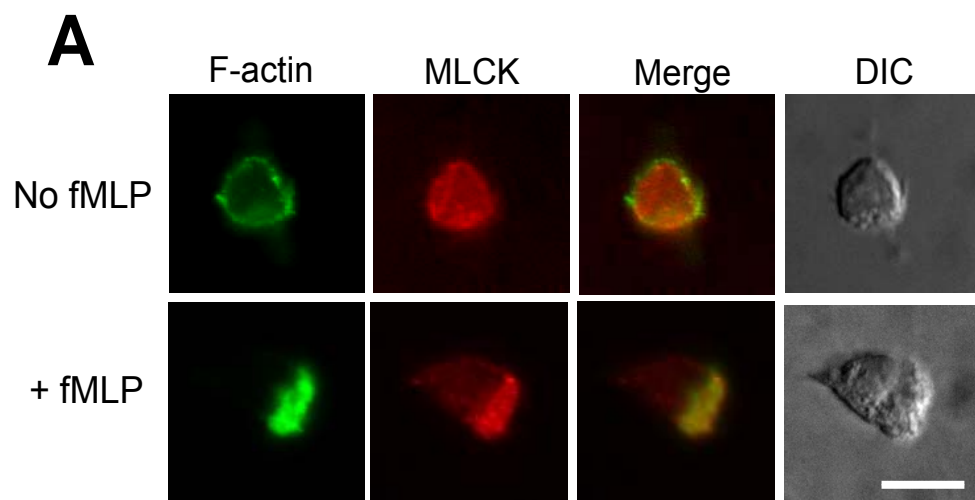


Figure 3

Figure 4

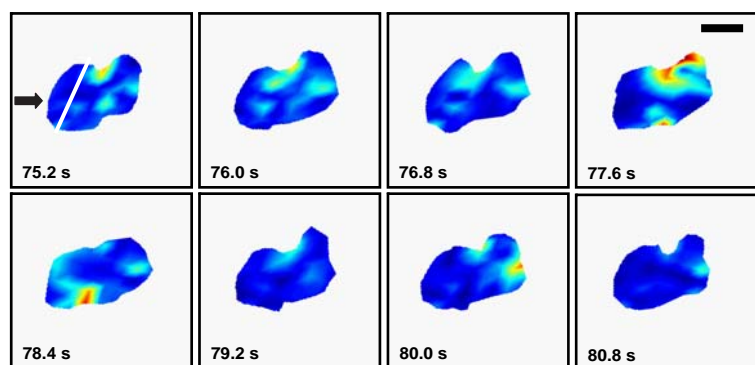
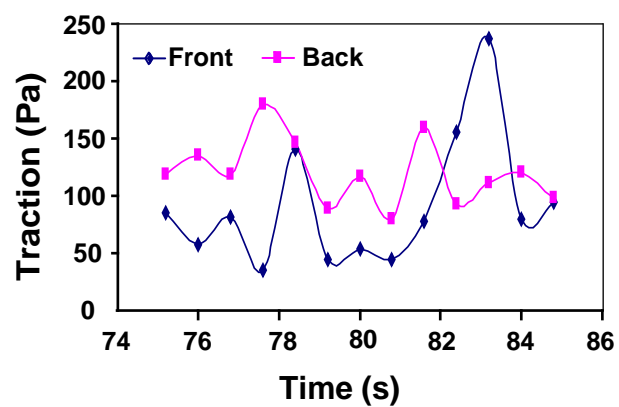
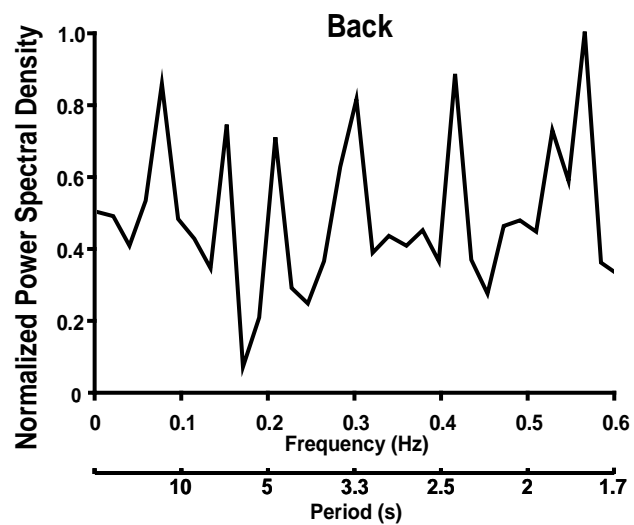
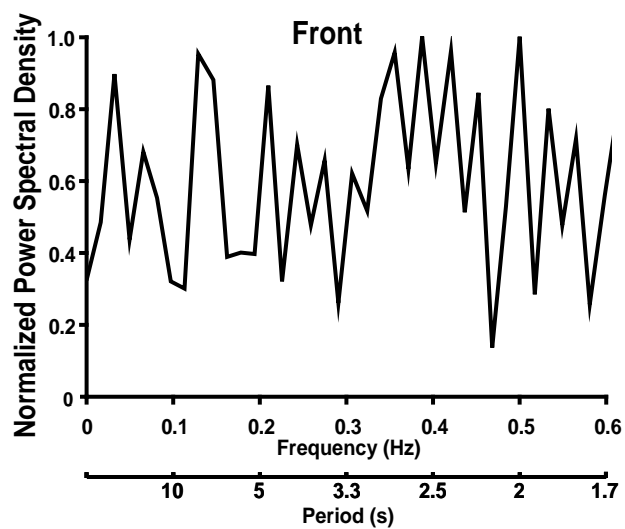
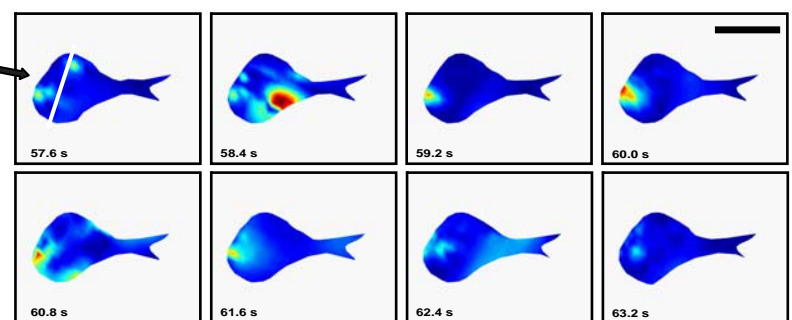
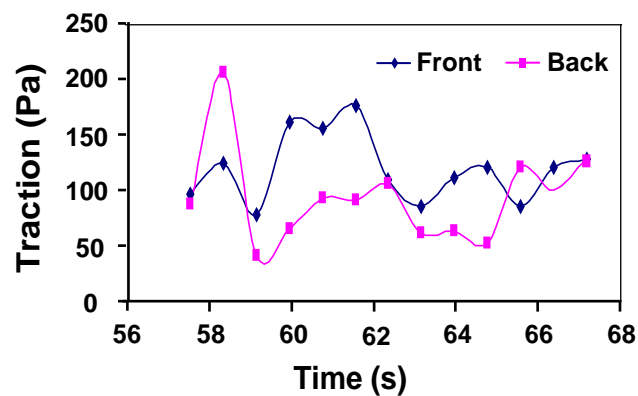
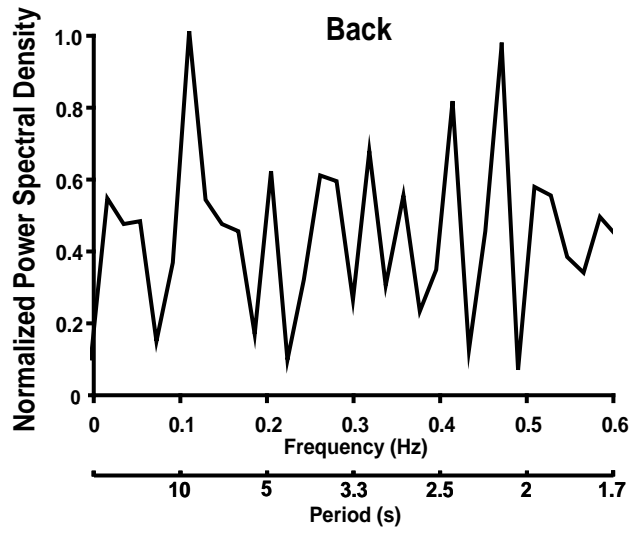
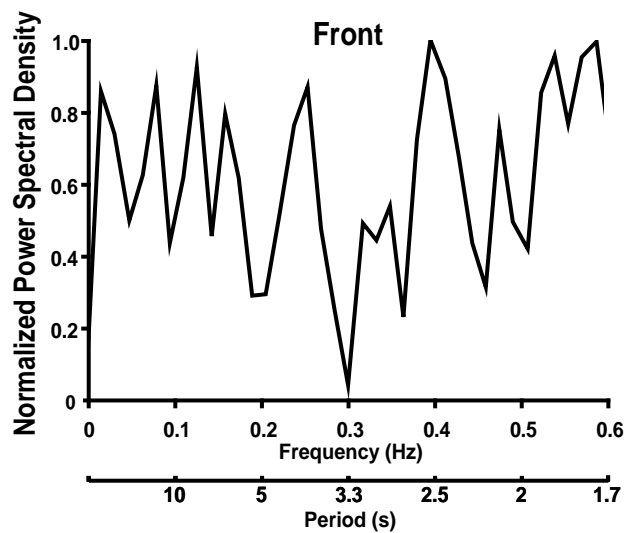
A**B****C****D****E****F**

Fig. 5

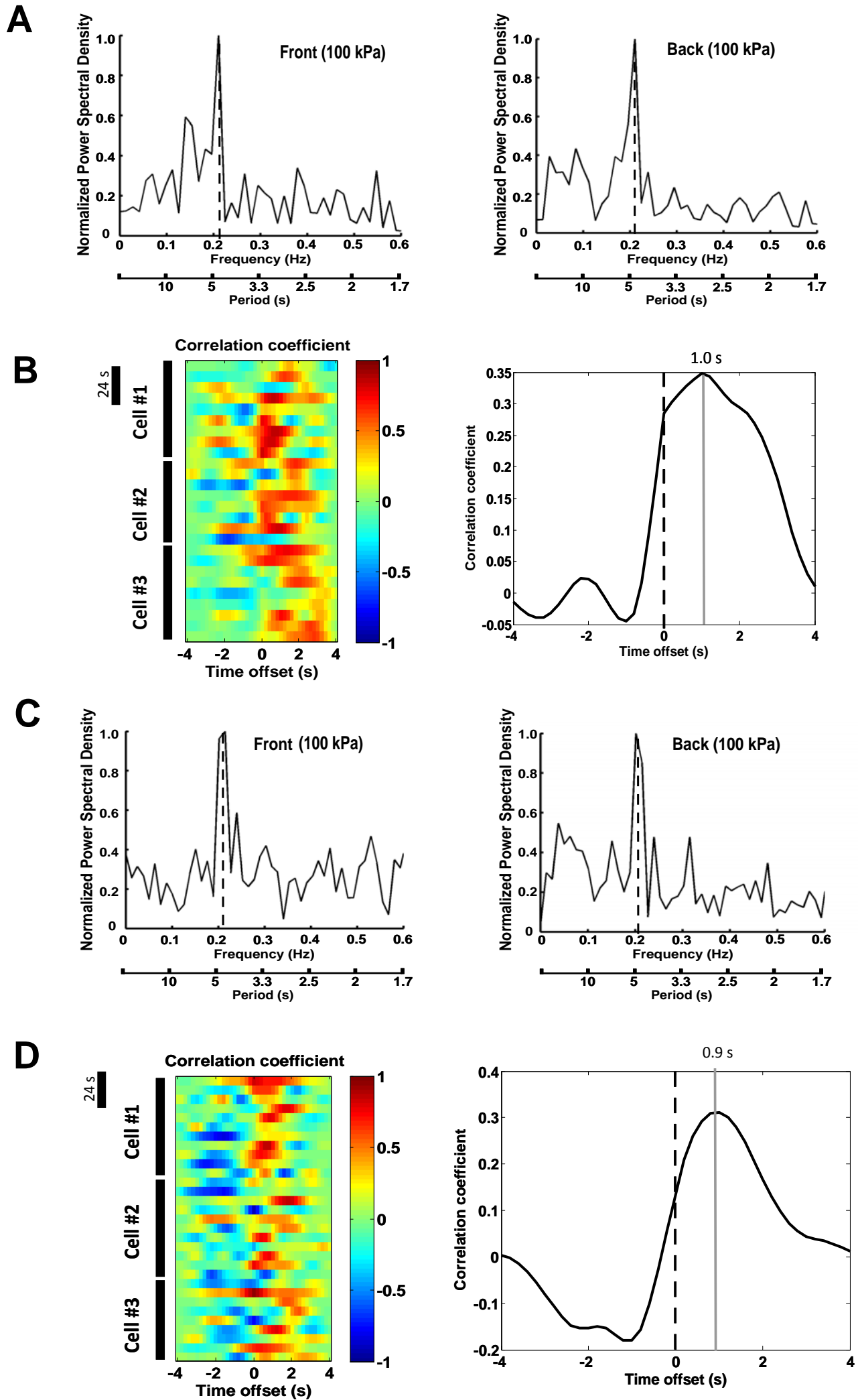
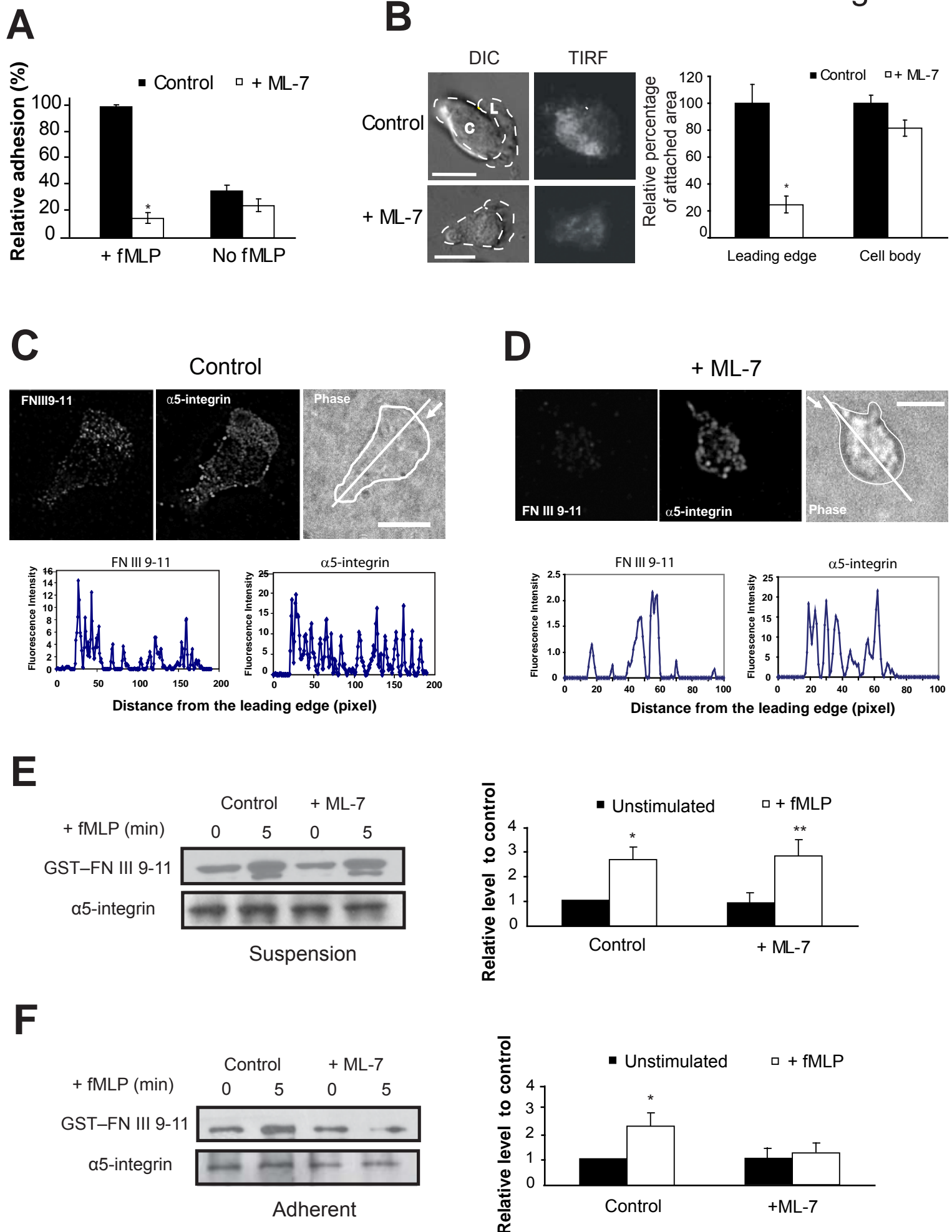


Figure 6



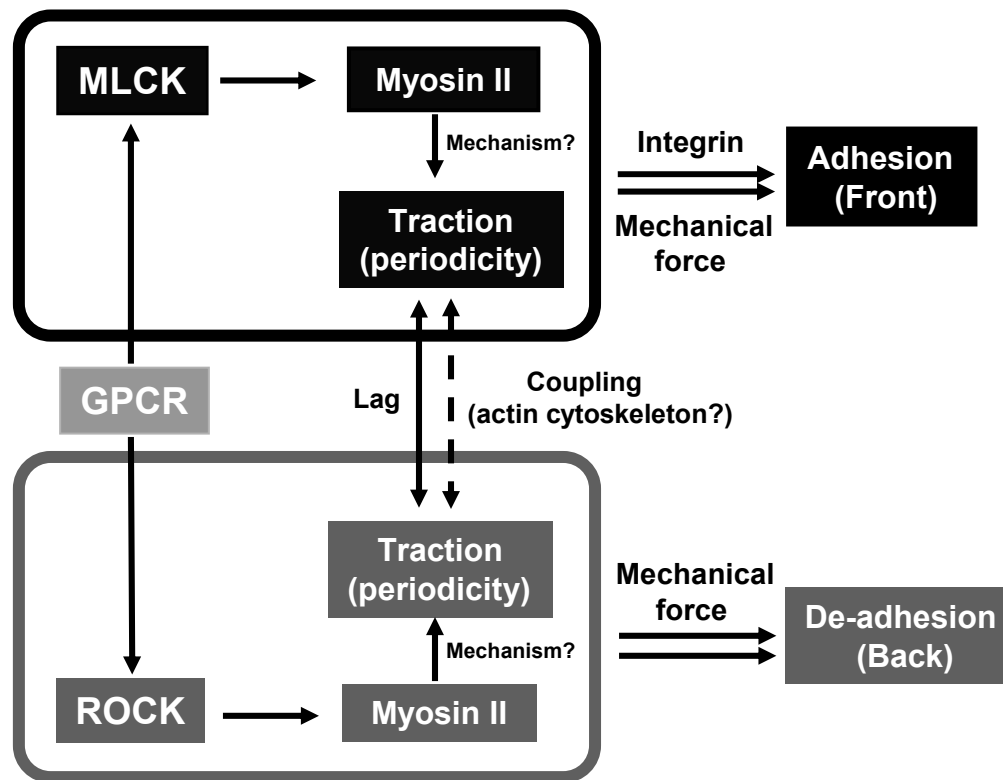


Figure 7